Hydrocarbon-derived ferromanganese nodules in carbonate-mud mounds from the Gulf of Cadiz: Mud-breccia sediments and clasts as nucleation sites

F.J. González [a,*], L. Somoza [a], R. Lunar [b], J. Martínez-Frías [c], J.A. Martín Rubí [a], T. Torres [d], J.E. Ortiz [d], V. Díaz del Río [e], L.M. Pinheiro [f], V.H. Magalhães [f]

[a] Geological Survey of Spain (IGME), C/Ríos Rosas 23, 28003 Madrid, Spain
[b] Departamento de Cristalografía y Mineralogía (UCM), C/José Antonio Novais 2, 28040 Madrid, Spain
[c] Centro de Astrobiología (CSIC/INTA), 29006 Torrejón de Ardoz (Madrid), Spain
[d] Laboratorio de Estratigrafía Biomolecular (ETSIM/UPM), C/Ríos Rosas 21, 28003 Madrid, Spain
[e] Centro Oceanográfico de Málaga (IEO), Apdo. 285, 29640 Fuengirola (Málaga), Spain
[f] Departamento Geociencias e CESAM, Universidade de Aveiro, 3800-193 Aveiro, Portugal

A B S T R A C T

More than 500 Fe–Mn nodules were sampled during the Anastasya-01 cruise (TASYO project) along the continental margin of the Gulf of Cadiz (eastern Central Atlantic), at the confluence of the Mediterranean Sea with the Atlantic Ocean, where extensive nodule fields were discovered. Based on wide previous studies that included swath bathymetry, multi-channel and very high-resolution seismic reflection, gravimetry, magnetism and underwater photography surveys, nodules were collected at water depths ranging from 850 to 1000 m, associated with hydrocarbon-derived ankerite and dolomite chimneys and crusts. Thirty six selected samples among the various morphological types were used for the laboratory analysis of physical properties (morphology, colour, surface texture, sphericity, weight and size), mineralogy (XRD, optical and electronic microscopy) and geochemistry (XRF, AAS, ICP-MS, EPMA, GC-MS, S, C and O isotopes). Nodules show a wide range of sizes, densities, weights and morphologies. Nodules are formed of multiple millimetre-thick layers of Fe and Mn oxyhydroxides surrounding the nucleus composed of Early–Middle Miocene plastic marl. The textures developed by the Fe and Mn oxyhydroxides layers are massive, laminated, detrital and mottled to dendritic. Goethite, lepidocrocite, Mn-oxides (7 Å-manganates and 10 Å-manganates), quartz, and phyllosilicates are the main components. Accessory minerals are calcite, dolomite, siderite, rhodochrosite, kutnohorite, pyrite, chalcopyrite, potassium feldspar, zircon, rutile, ilmenite, and chlorite. Fe–Mn carbonates from the siderite–rhodochrosite continuous series are forming part of the marl nuclei. Framboidal, filamentous, and globular textures are observed in Fe–Mn oxides and pyrite suggesting biogenic origin. Nodules show a high mean abundance of Fe (38.6%) moderate Mn (6.0%), and low contents of trace metals and REEs compared to the average content of deep-seabed polymetallic nodules from other oceanic areas. The Mn/Fe ratio ranges from 0.07 to 0.25. The studied nodules hold in their oxide layers hydrocarbons (n-alkanes) derived from marine bacterial activity. Aromatic hydrocarbons in the form of phenanthrene, are also present which is characteristic of mature petroleum. The structure, mineralogy, and chemical composition in the studied nodules are similar to those of diagenetic–hydrogenetic continental margin nodules rather than deep-sea nodules. We suggest that the formation of this type of nodule occurred through a combined diagenetic–hydrogenetic growth process involving fluid venting from deep-seated hydrocarbon reservoirs, bio-mineralization processes, and bottom current erosion.

1. Introduction

Polymetallic nodules were first discovered in 1868 in the Kara Sea, Russia (Murray and Renard, 1891). With the advance of underwater exploration techniques during the 1960s and 1970s, seabed polymetallic nodules were considered a potential economic resource of great interest (Rona, 2002). Deposits of Fe–Mn nodules are distributed in all the oceans of the world, although there are some areas where they are especially abundant or rich in elements of economic interest, such as the Clarion–Clipperton Fracture Zone in the northeast Pacific Ocean, the Central East Indian Basin in the Indian Ocean and the Peru Basin in the south-eastern Pacific Ocean (e.g., Cronan, 1977; Rona, 2003). During the last four decades, the prospecting and research for polymetallic nodules and crusts has been very active (e.g., Glasby, 1977; Nicholson et al., 1997; Dekov and Savelli, 2004; Verlaan et al.,

2005). Because of this, in 2000 the International Seabed Authority (ISA) approved regulations and environmental guidelines on exploration for polymetallic nodules in the area of the seabed beyond national jurisdiction (ISA, 1999, 2000).

The existence and extent of seabed resources in the Gulf of Cadiz (Fig. 1) was unknown until the advent of such technologies as multibeam bathymetry echosounders and long-range side-scan sonars for deep marine exploration. Several cruises were carried out aboard the research vessels *Prof. Logachev*, *Hespérides*, and *Cornide de Saavedra* from 1999 to 2006 in the Gulf of Cadiz. Cooperation between the IOC-UNESCO "Training Through Research" TTR cruises and the "TASYO" project led to the discovery of large fields of fluid venting structures in the Gulf of Cadiz such as mud volcanoes bearing gas hydrates (Ivanov et al., 2000; Gardner, 2001; Somoza et al., 2002), ankerite and dolomite chimneys, nodules, crusts and slabs (Somoza et al., 2003; Díaz-del-Río et al., 2003; Magalhães et al., 2005; León et al., 2006), and more recently, Fe–Mn nodules (González, 2004; González et al., 2006a, 2007) associated with these structures in this tectonically active area.

Here we present underwater images and detailed physical, textural, mineralogical, and geochemical descriptions of the Fe–Mn nodules that were recently discovered along the continental margin of the Gulf of Cadiz. The nodules are associated with hydrocarbon-related seeps. In addition, we present a comparative analysis with other deep-seabed polymetallic nodules, shallow-water and continental margin nodules from other ocean basins and tectonic settings of the world.

2. Geological setting

The Gulf of Cadiz is located at the westward front of the Betic–Rifian Arc, in the easternmost sector of the Azores–Gibraltar segment

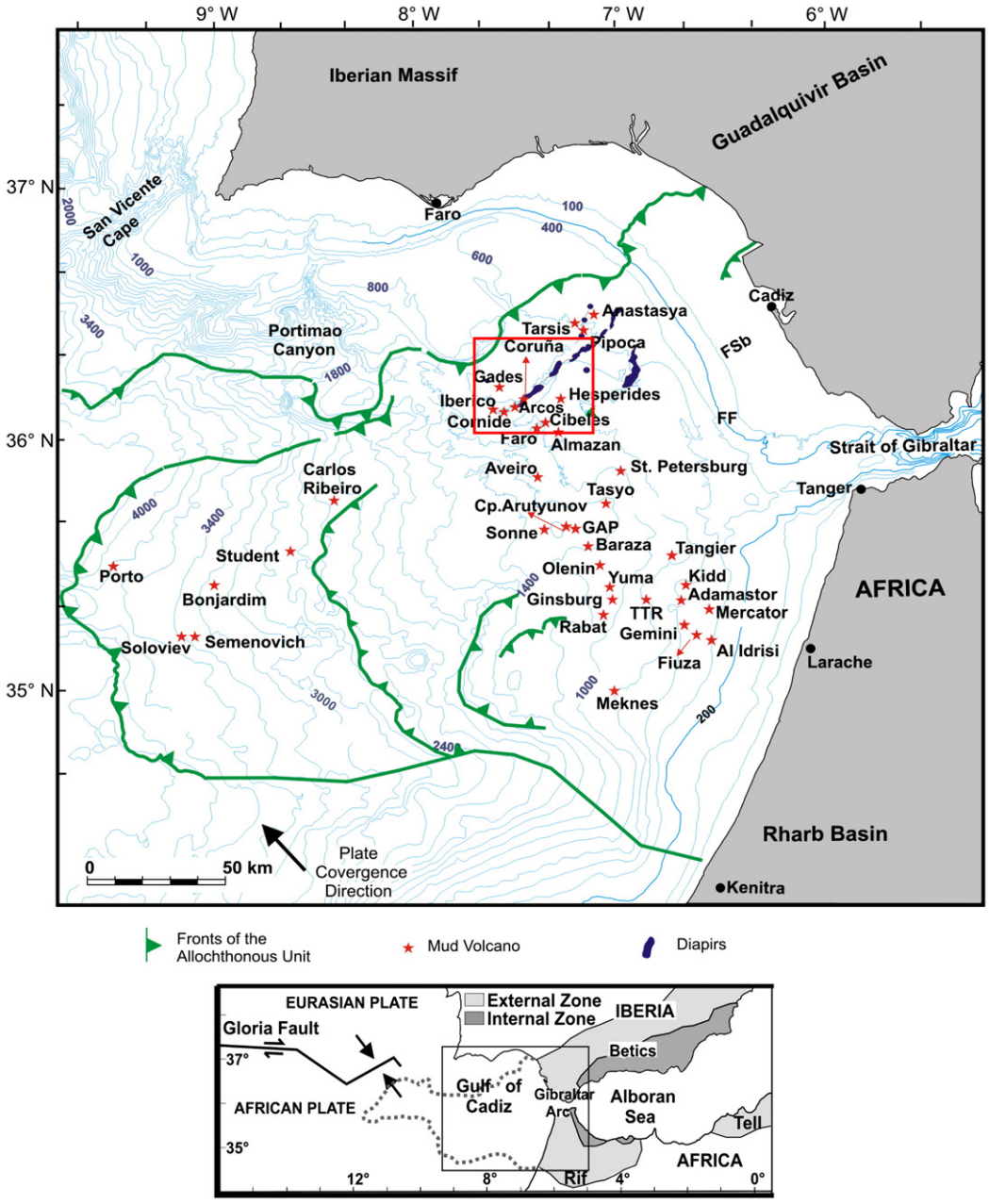

Fig. 1. Geological setting and simplified bathymetry of the Gulf of Cadiz. The rectangle marks the location of the nodule fields in the Guadalquivir Diapiric Ridge area (GDR). Bathymetry in meters. Partially modified from León et al. (2006).

of the Africa/Eurasia collisional plate boundary (Dewey et al., 1989) (Fig. 1). It has a complex geological history and has undergone several episodes of rifting, compression, and strike–slip motion since the Triassic (Maldonado et al., 1999). In late Tortonian times (7.1–11.2 Ma), a large sedimentary body was emplaced in the Gulf of Cadiz, caused by westward migration of the Alboran domain associated with the formation of the Betic–Rifian Arc (Bonnin et al., 1975; Auzende et al., 1981; Lonergan and White, 1997; Maldonado et al., 1999). During the final stages of accretion of the Betic–Rifian Arc and the emplacement of thrusting units, gravitational sliding of mobile shale and salt stocks formed a giant complex of mass-wasting deposits, generally known as the "*Gibraltar Olistostrome*", that reached as far west as the Horseshoe and Seine abyssal plains. This feature appears as a chaotic, highly diffractive body, with high-amplitude reflections on seismic sections (Riaza and Martínez del Olmo, 1996) and it consists of a mixture of Triassic, Cretaceous, Paleogene, and Neogene sedimentary units, overlying Palaeozoic basement (Maldonado et al., 1999). It involves a huge volume of mud and salt diapirism of Triassic salt units and undercompacted Early–Middle Miocene plastic marls (Maestro et al., 2003). The origin of this chaotic body is highly controversial. It has been interpreted as a complex of olistostromes and debris flows, originated by gravitational sliding, and tectonic thrusted units – tectonic *mélanges* (Torelli et al., 1997; Maldonado et al., 1999; Medialdea et al., 2004). Alternatively, it has also been interpreted as an accretionary complex related to the migration of the Alboran terrain as a consequence of a once active subduction zone (Royden, 1993). Recently, Gutscher et al. (2002) proposed that this subduction is still active beneath Gibraltar.

Throughout this area, extensive hydrocarbon-rich fluid venting and mud diapirism are observed, which includes numerous mud volcanoes, methane-related authigenic carbonates (crusts, chimneys and carbonate mounds) and pockmarks (Baraza and Ercilla, 1996; Ivanov et al., 2000; Gardner, 2001; Díaz-del-Río et al., 2003; Pinheiro et al., 2003; Somoza et al., 2003). These are related to the lateral compression from Africa–Eurasia convergence, which promoted fluid migration via deep-seated faults to the surface. Several NE–SW oriented diapiric mud ridges have been found in the NE sector of the Gulf of Cadiz, which are characterised by abundant carbonate chimneys and crusts on top of the ridges (Díaz-del-Río et al., 2001; Somoza et al., 2003; Fernández-Puga, 2004). Focal mechanism solutions show that the stress regime along the Africa–Eurasian plate boundary in this area is a combination of dextral strike–slip and a NW-directed compression near Gorringe Bank and the Gulf of Cadiz (Borges et al., 2001). Presently, the direction of maximum horizontal compressive stress along this segment of the plate boundary is estimated to be approximately WNW–ESE in the Gulf of Cadiz, leading to a general transpressive regime in this area (Cavazza et al., 2004).

Outflow of the Mediterranean waters from Strait of Gibraltar towards the Atlantic Ocean, causes region specific erosive, biotic and temperature conditions over the seabed. The Mediterranean Outflow Water (MOW) crosses the Strait of Gibraltar and is channelled through existing submarine channels from 600 to 1200 m water depth along the continental slope of the Gulf of Cadiz (Hernández-Molina et al., 2003).

3. Methods

3.1. Data acquisition and swath bathymetry

Data presented here were acquired during the oceanographic cruises Tasyo/2000 and Anastasya/2000/2001 aboard the research vessels "*Hespérides*" and "*Cornide de Saavedra*". The study area (8500 km^2) was extensively surveyed with swath bathymetry, multi-channel and very high-resolution seismic reflection, gravimetry, magnetism, underwater cameras, dredging, and gravity coring. Navigation was by differential Global Positioning System (DGPS) for which the average navigational accuracy is estimated to be better than 5 m. A multibeam echo-sounder EM12S-120 was operated at a main frequency of 13 kHz, with 81 beams, which allowed a maximum coverage angle of 120° (about three times the water depth). This system, triggered with a range of pulse lengths from 2–10 ms, has a vertical resolution of 0.6 m. A bathymetric map, contoured at an interval of 10 m and a seafloor backscatter image was generated (León et al., 2001) from the data. A dense network of parametric echo-sounder TOPAS (Topographic Parametric Sound) and Sparker seismic data were collected. TOPAS uses chirp wavelets, operating at two simultaneous primary frequencies, 15 and 18 kHz. Through the parametric effect in the water, a secondary frequency is produced in the range of 0.5–5 kHz. Penetration of up to 100 m was obtained with a resolution of 0.5–1 m. Sparker data (50 Hz–4 kHz) were collected during cruises Anastasya-99 and Anastasya-00 with an energy source ranging between 3500 and 7000 J and a recording length of 2s TWT. Submarine photographs were taken with a *Benthos-372* underwater deep-sea camera during the cruise Anastasya-01 after detailed bathymetric surveys. The seabed images were very useful in order to establish the relationships between seabed structures and to identify targets for dredging and coring. Twenty dredges (benthic type) and 22 gravity cores were taken along a sector determined from bathymetric, seabed reflectivity, and magnetism maps.

3.2. Sampling and geochemical, mineralogical and isotopic analyses

The Fe–Mn nodules were collected from the Gulf of Cadiz at the Guadalquivir Diapiric Ridge area (GDR) (Figs. 1 and 2). They were recovered during cruise Anastasya/2001 aboard the research vessel "*Cornide de Saavedra*" using rectangular benthic dredges. Previously collected dredges, bottom photograph surveys, and sediment core samples indicate the presence of Fe–Mn nodules within an area of high backscatter on sidescan sonar maps. The samples recovered are comprised of 561 Fe–Mn nodules with a total weight of 36.6 kg. These were classified into different groups based on their superficial colour, external morphology and size. 46 selected samples from distinct nodule types were studied at the "Centro de Astrobiología" (CAB/CSIC), "Centro de Microscopía Electrónica Luis Bru" at the Complutense University of Madrid (UCM), the "Laboratorios del Instituto Geológico y Minero de España" (IGME), the "Laboratorio de Estratigrafía Biomolecular" at the Polytechnic University of Madrid (UPM) and the "Servicio General de Isotopos Estables" at the University of Salamanca (USAL) using the methods outlined below.

Selected samples were cut vertically in two halves with respect to their position on the seafloor. One half was used for the present study and the other was retained by the Geological Survey of Spain. The samples were first thoroughly examined by transmitted and reflected light microscopy, and the internal structure was described, outlined and photographed. In all, 29 polished sections, 24 thin sections and 46 polished specimens were examined. Apparent wet bulk density and open porosity were determined by water absorption in void according to the UNE-EN 1936:1999 normative. Real dry bulk density was calculated by the helium pycnometer method with an Accupyc 1330 pycnometer. Multielemental punctual analyses and mapping profiles were carried out in areas of interest determined by petrographic studies, using electron probe micro analysis (EPMA) with a JEOL Superprobe JXA-8900 M, operating at 20 kV and 50 mA, fitted with wavelength dispersive spectrometers (WDS). Back-scattered electron images were also obtained with this instrument. Standards included pure metals, synthetic and natural minerals all from international suppliers. Scanning electron microscopy (SEM-EDS) of morphological and 3D textural mineral characteristics was performed on a JEOL JM-6400 instrument. Individual layers of special interest for geochemical, mineralogical and growth rates determinations were sampled under the microscope with a needle drill. Bulk mineralogical X-ray diffraction (XRD) profiles from $2q = 2–60°$ in 0.005 steps were obtained in 25

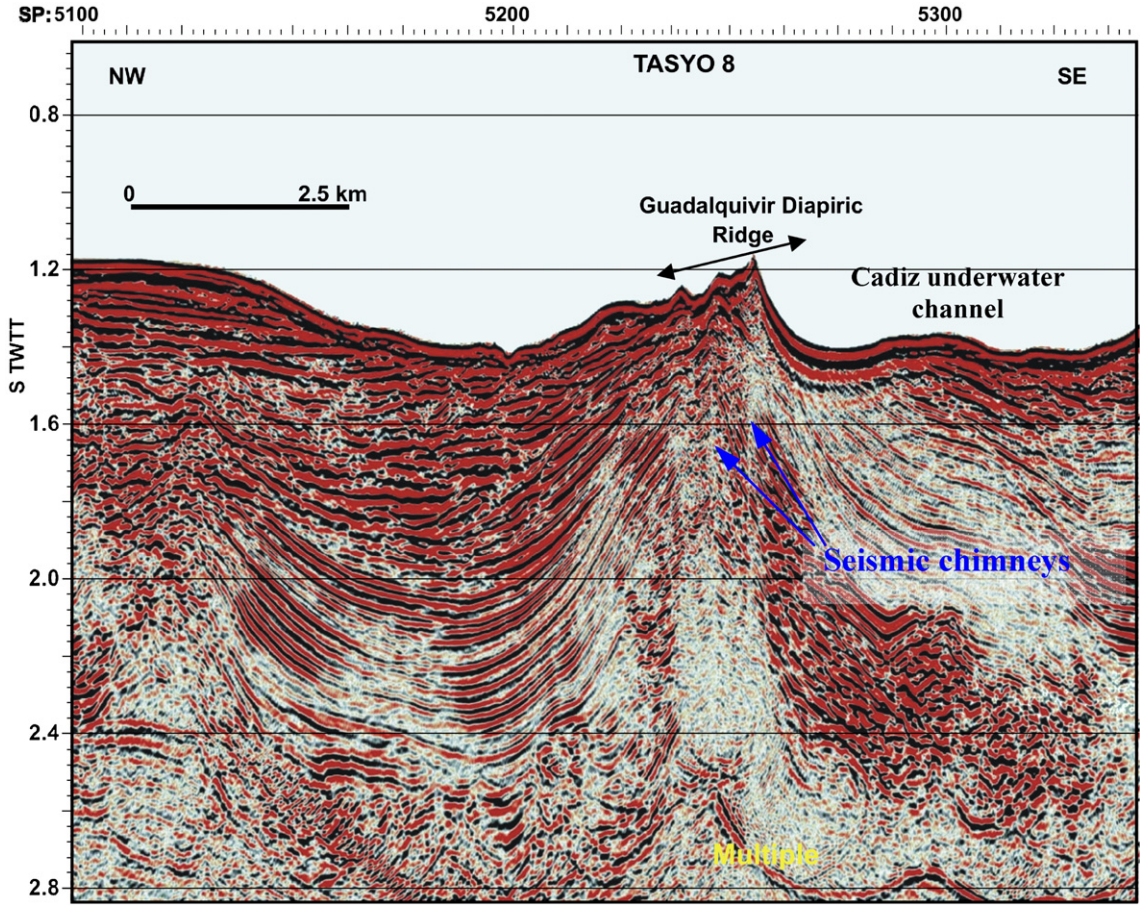

Fig. 2. NW–SE multichannel seismic profile showing the GDR carbonate-mud mounds with an internal chaotic and indistinct seismic reflection pattern and development of "seismic chimneys". A suite of more than 500 Fe–Mn nodules were collected on the flanks of these mounds. Double arrow indicates location of Fe–Mn nodules fields.

samples using XPERT PRO of PANalytical, Cu-Kα radiation (35Kv, 40 mA) with graphite monochromater, software *High Score* and ICDD data base. 35 bulk nodules were measured for major (Al, Fe, Mn, Ca, Mg, Si, K, Ti and P) and trace elements (Sc, V, Cr, Co, Ni, Cu, Zn, Pb, Sr, Ba, Br, Rb, Zr, Th, U, As, Mo) by X-ray fluorescence (XRF) using a MagiX of PANalytical instrument with Rh radiation. B was calculated by induced coupled plasma atomic spectrometry (ICP-AES). Au, Na and Li were measured using atomic absorption with a VARIAN FS-220. The growth rate (GR) of the nodules was calculated by the *Co chronometer* method, derived by Manheim and Lane-Bostwick (1988). Studies on marine ferromanganese nodules have suggested a relationship between growth rate and chemical composition (e.g., Reyss et al., 1982). The suggestion is based on the hypothesis that the metals in nodules have two sources of supply: bottom seawater (hydrogenous) and sediment pore water (diagenetic). Following this assumption, the Co method (cobalt chronometer) is normally used to determinate age in Fe–Mn concretions based on the relationship between Co content and growth rate. Various authors have established equations to calculate growth rate, and one of the most accepted is the equation proposed by Manheim and Lane-Bostwick (1988):

$$\text{Growth rate}\left(\text{mm Myr}^{-1}\right) = 0.68 / \text{Co}_{\text{w}}^{1.67}$$

where, Co_{w} is the Co concentration in wt.% less detrital background concentration of 0.0012 wt%.

One limitation of this method is that the equation does not take into account the possible hiatuses during the accretion process. Therefore, the calculated rates represent maximum values and the derived age minimum values (Hein et al., 1990). Loss on ignition (LOI) was determined by calcination at 950 °C and S was measured in ELTRA CS-800 equipment. The bulk REE concentrations of selected samples were determined by induced coupled plasma mass spectrometry (ICP-MS-TOF) in a RENAISSANCE instrument. TOC was made for 14 bulk nodules by subtracting the TIC obtained by calcination at 550°C, from the TC values and measured in ELTRA CS-800 equipment. Biomarkers were analyzed by combined gas chromatography-mass spectrometry (GC-MS). Component identification was based on comparison of the mass spectra and the GC retention times with published data from reference compounds. C and O isotopes measurements were carried out by fractionated extraction of carbon dioxide (Walters et al., 1972; Al-Aasm et al., 1990) with 103% phosphoric acid at 25°C/3 h in calcite and 25°C/3 days in dolomite. Isotopic ratios were measured in a SIRAII VG-Isotech mass spectrometer. For sulphur isotope analyses SO_2 was extracted from pyrite by void combustion in the presence of Cu_2 O according to Robinson and Kusakabe (1975) and Coleman and Moore (1978) methodologies, and measured in a SIRAII VG-Isotech mass spectrometer. The reproducibility of the analytical procedure was better than 0.1‰ for sulphur, carbon and oxygen.

The inter-element associations were determined using SPSS-13 software, and only the significant associations ($r \geq 0.35$ at 95% and 99% confidence level) are used.

4. Results

4.1. The GDR nodule fields and their distribution on the seafloor

Nodule fields extend in a region along the middle continental slope at an average depth of 900 m. The most prominent physiographic features of this sector are: a) a NE–SW diapiric ridge with a vertical relief of 300 m named Guadalquivir Diapiric Ridge (Somoza et al.,

2003) and, b) the Cadiz Channel through which the Mediterranean Outflow Water (MOW) undercurrent circulates. Several individual mounds were identified along the Guadalquivir Diapiric Ridge. Dredge hauls from the top of these mounds yielded large amounts of carbonate crusts, chimneys and mud-breccia flow deposits composed mainly of ejected materials, mostly Miocene marls and muds. Indications of gas saturation include degassing structures, the presence of hydrogen sulphide (H_2S), and chemosynthetic fauna (*Pogonophora* sp. tube worms, *Calyptogena* sp. and *Acharax* sp.). The fields of Fe–Mn nodules occur at the base of the mounds, where the influence of the MOW is strong and where rippled seabed and carbonate crusts and chimneys also occur (Fig. 3). The underwater images show a variable density of nodules overlying the seafloor, from 3% to 75%, fundamentally together with carbonate chimneys and crusts. Commonly the nodules occur in a patchy distribution on the seabed and are characterised by tabular-irregular morphologies, absence of incrusting benthic organism, and are black in colour. The surface sediments in the nodules fields are highly oxidized and brown in colour, but the subsurface sediments, only a few centimetres below, are olive-grey muds and silts containing H_2S and pyrite.

4.2. Fe–Mn nodules: morphology, sizes, surface features and physical properties

The nodules of the Gulf of Cadiz display differing morphological types: tabular, irregular, discoidal, sub-spherical, ellipsoidal, and cylindrical, but the most abundant type is the tabular morphology (Fig. 4). Tabular to irregular samples represent more than 90% of the nodules recovered. The surface texture is smooth to rough, and botryoidal. Edges of nodules normally are rounded. Superficial carbonate encrustations of tube worms and bryozoans are common with rare occurrences of small corals. Unlike the carbonate chimneys and crusts, the nodules do not exhibit superficial boring by benthic organisms. The surface colour varies between light orange and black, is independent of the size or shape of the nodule, and reflects the fundamental chemical composition of the external part of the samples: iron oxyhydroxides (orange to red colour) and manganese oxides (black colour). Fractures with differing directions, greater than 1 mm wide, and variable length are visible in their surface, especially in big nodules. These fractures can be open or filled with bottom sediment and mineral precipitates. The maximum diameter of the nodules varies between 1.6 and 20.4 cm, weight is between 1.37 and 1818.8 g, porosity between 23.9 and 44.3% in volume, and dry bulk density between 3.3 and 3.5 g/cm^3.

4.3. Internal structure

The structure of a whole nodule is best revealed by photographs in megascopic polished sections in hand samples. We can distinguish three different structural elements in the nodules studied in this work: nucleus, layers and discontinuities.

4.3.1. Nucleus

Nodule growth always starts at a nucleus with variable degree of hardness. A total of 46 polished nodules revealed more or less clearly their nucleus. Samples with one or several cores (polinucleated) (Fig. 4B, E) and samples composed by the accretion of several nodules (polinodules) (Fig. 4A) exist. We can distinguish two extreme kinds of nuclei in relation with their nature: nuclei composed of soft sediment (Fig. 4B,D) with diffuse limits and nuclei composed of hard marl clasts with tabular morphology and well defined angular exterior edges (Fig. 4A). Both types of cores generally are impregnated by Fe–Mn oxyhydroxides, especially the nuclei composed of soft sediment. Nucleus colour is beige and orange to red when it is impregnated by oxides. Millimetric veins of oxides and signs of burrowing appear crosscutting some soft nuclei. The size of the core ranges from 1 mm to 4.5 cm. The nucleus can be situated in the central or lateral position in the sample with symmetric or asymmetric distribution of Fe–Mn layers around it respectively. The exterior shape of the nodule frequently reflects the shape of the nucleus. The small nodules, less than 2 cm in maximum diameter, have very small cores and result in spherical to sub-spherical nodules (Fig. 4F,G,H,I). Big samples

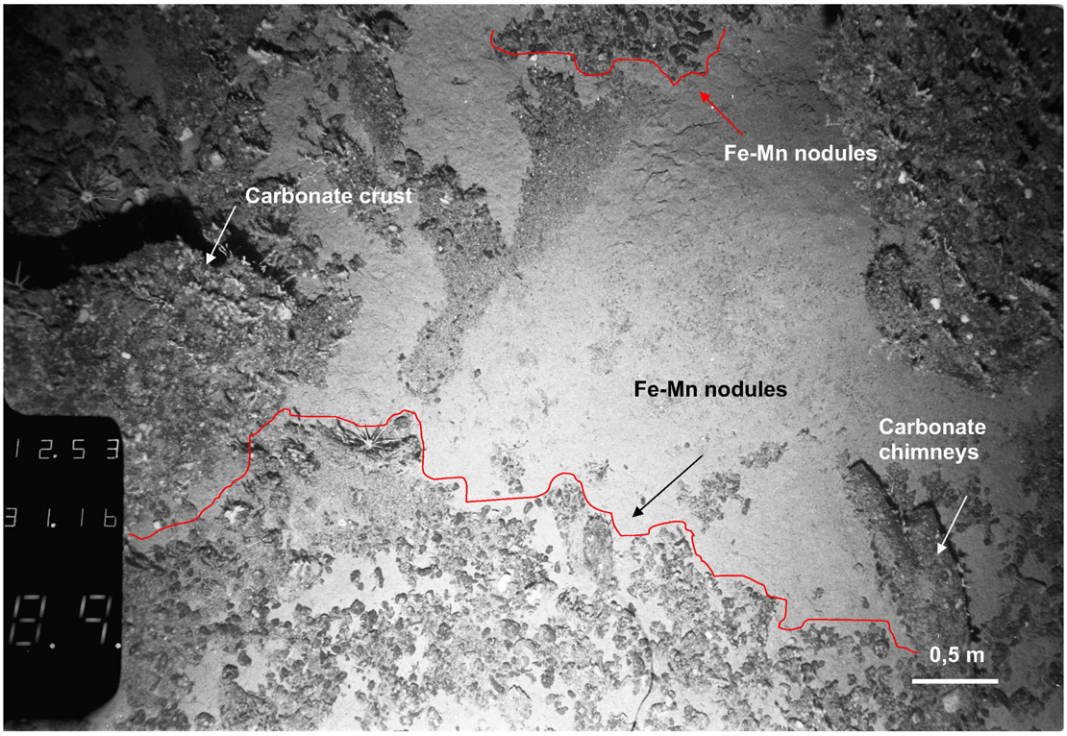

Fig. 3. Underwater image showing Fe–Mn nodules lying on the seabed. They were photographed near the Guadalquivir Diapiric Ridge area (see rectangle in Fig. 1). Nodules in patchy distribution are close to hydrocarbon-derived carbonate slabs covered by deep corals, sponges, and echinoids. Two carbonate chimneys are also observed lying on the seabed.

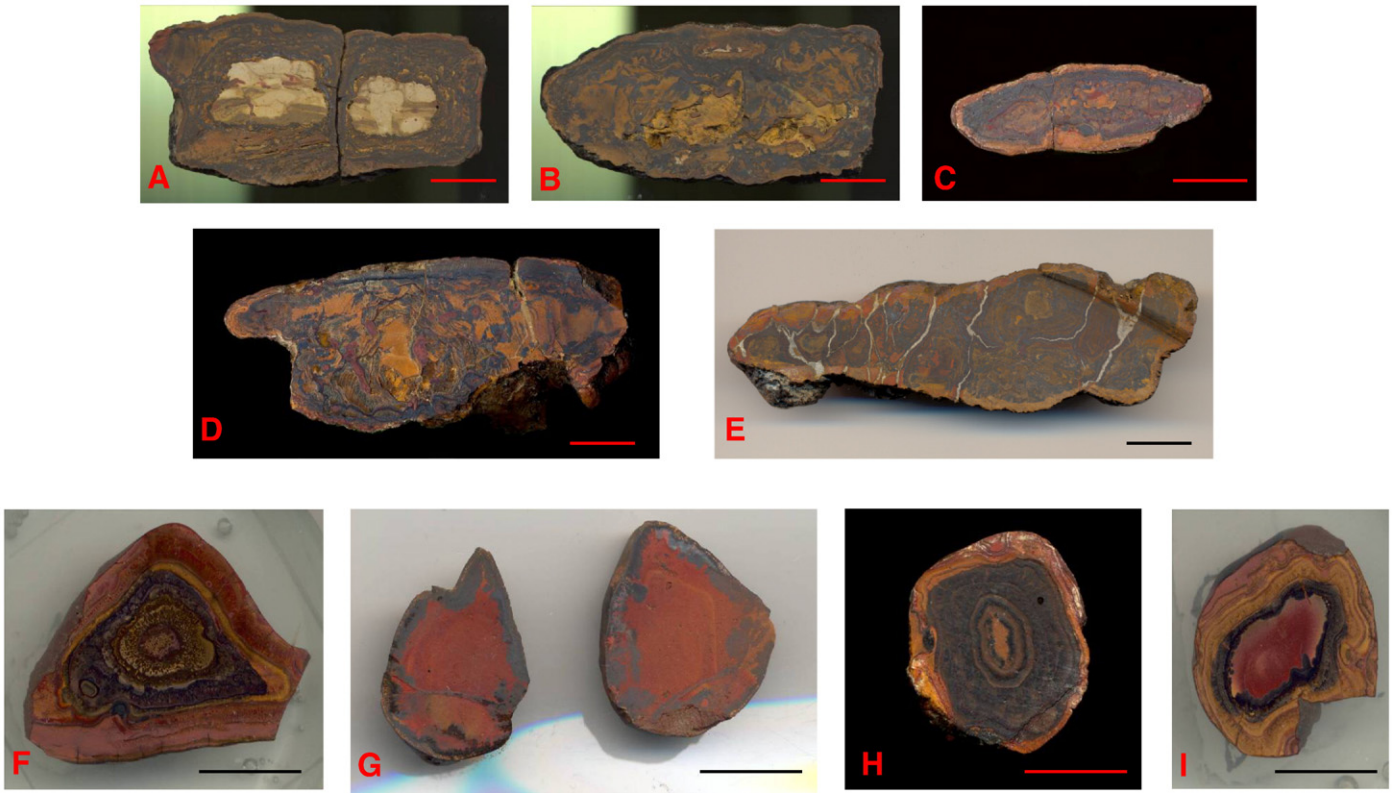

Fig. 4. Sections of different morphological types of nodules showing the most typical macroscopic internal features. Tabular to irregular big nodules are showed in the images A, B, C, D and E. The photographs F, G, H and I show sub-spherical to spherical small nodules. Scale bar represents 1 cm.

normally have large nuclei, commonly tabular, and result in tabular to irregular shaped nodules (Fig. 4A,B,C,D,E).

4.3.2. Layers

The nodules from the Gulf of Cadiz are characterised by layered growth. They show dark colours or even opaque from yellow to black. The periodic growth of the nodules can be reflected by a well expressed concentric fabric, especially in small samples, which frequently presents a succession of black layers (in which Mn-oxides predominates) and yellow or brown ones (fundamentally with Fe-oxides). The nodules are practically always composed of both elements, but depending upon the conditions of formation, one of them dominates. Nodules <2 cm in diameter have symmetric distribution of growth layers, but larger samples display an asymmetric and complex growth pattern. Four different types of internal growth structure are identified: laminated, massive, mottled to dendritic, and detrital (Fig. 5). The laminated structure is characterised by the development of sub-parallel successions of iron (yellow to brown) and manganese rich layers (black), which are very continuous laterally. The borders of layers are sharp or diffuse and the thickness is from 2 μm to 600–700 μm. The massive structure is composed of millimetric areas containing a mixture of finely crystalline Fe–Mn oxides without differentiable layers. They have a compact appearance with brown to black colours. Mottled to dendritic structure is defined by specks from 10 μm to 500 μm of goethite (brown in colour) with rounded to elongated morphology surrounded by a mixture of phylosilicates, carbonates and Fe–Mn oxides (yellow to orange). Mottled and dendritic areas generally are in continuity. In some cases the mottles are composed of Mn-oxides and the dendritic structure associated is formed by very rich manganese minerals. Frequently these Mn-rich dendritic structures are related to fractures and early diagenetic processes. The detrital structure is characterised by the abundance of detrital angular grains (see Mineralogy section) forming continuous layers with thicknesses from 1 to several millimetres. These detrital layers seem to be overprinted by the concentric oxide layers. Detrital grains are impregnated by Fe–Mn oxides that surround and cement these. A detailed study of the layers and their mineral textures are described in the mineralogy section.

4.3.3. Discontinuities

When the normal development of growth layers is disturbed, we can define a discontinuity element. The nodules studied present five kinds of discontinuities easily visible in megascopic observations: fracture discontinuities, growth discontinuities, burrowing discontinuities, fluidification discontinuities and discontinuities of alteration. Fracture discontinuities have millimetric to centimetric longitude and are millimetric wide, frequently filled with detrital sediment and precipitates of carbonates and Fe–Mn oxides (Figs. 4A,D,E, 6F). The discontinuities have developed in perpendicular or in parallel to the Fe–Mn growth layers, frequently marking accretion limits between different nodules in composed samples (Fig. 4A). Unconformities in the growth pattern can be produced by a hiatus in the accretion history of the nodule. Fluidal structures are observed in big samples and are probably related to fluid migration (Fig. 4B). Burrowing discontinuities, due to benthic fauna excavation, are present in some big nodules (Fig. 4D). They have tubular morphology, are filled with detrital sediment and Fe–Mn precipitates. Most of the nodules studied present an external alteration front (discontinuity of alteration front) which affects 2–5 mm of the exterior layers, is orange to yellow in colour, has high porosity, and represents a post-depositional modification of the nodules (Fig. 4B,C,E,H,I).

4.4. Mineralogy

The mineralogy of iron–manganese marine deposits is very important because it reflects the genetic conditions during generation and, partly determines chemical composition. Most Fe–Mn minerals in the studied nodules lack an intensive difference in colour under

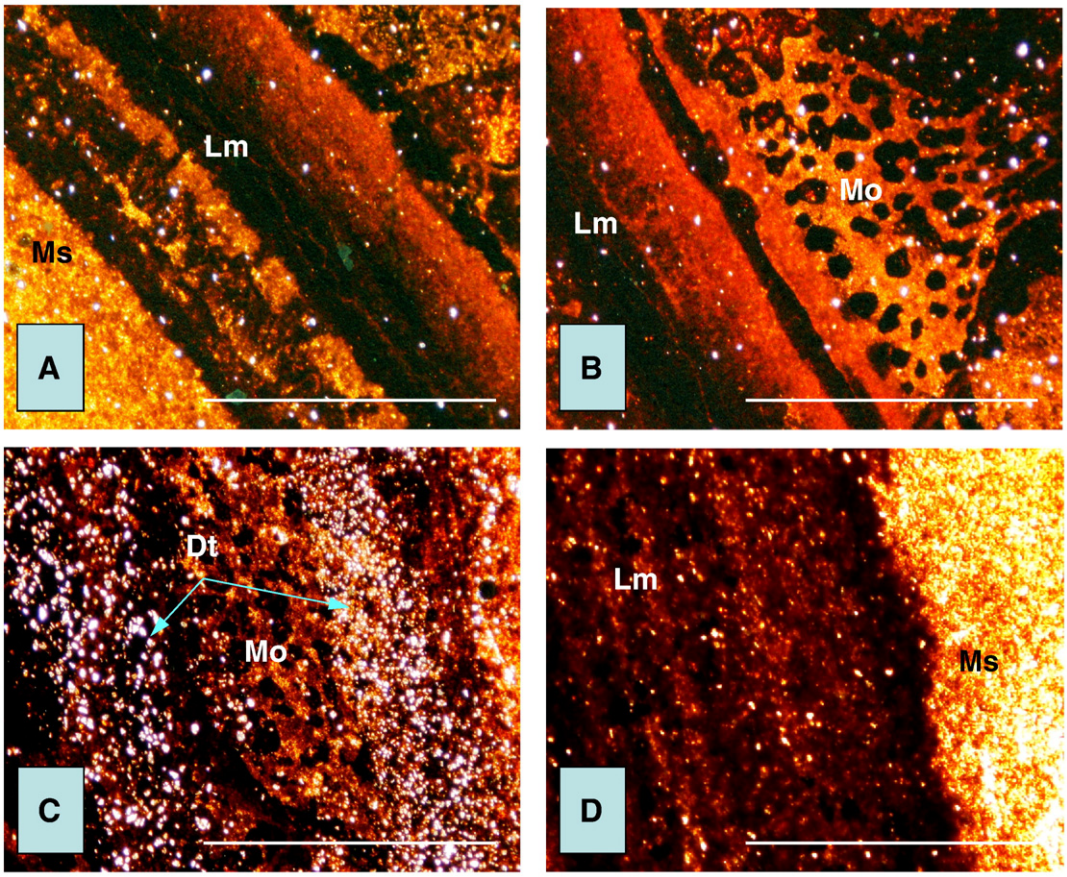

Fig. 5. Photomicrographs in transmitted polarized light. Four of the structures most characteristic of the studied nodules are observed: the laminate (Lm), massive (Ms), detrital (Dt) and the mottled (Mo). Scale bar represents 1 mm.

optic microscope, but they differ in reflectivity from white to dark grey. Typical interlamination of iron-rich layers (grey reflectivity) and manganese-rich layers (light grey to white) are present, especially in small nodules. Most nodule material, particularly iron and manganese oxides, is cryptocrystaline to amorphous and generally is closely intergrown. It is very difficult to distinguish optically Fe and Mn oxides without previous identification by XRD analysis of microsamples where frequently Fe–Mn oxides are intergrown. Minor quantities of silicates and other minerals (carbonates, sulphides) are present in the studied nodules. Transparent minerals commonly appear in two different ways: dispersed and in continuous layers very rich in detritals (detrital structure) and poor in Fe–Mn oxides. Most nodules contain a large proportion of very low crystalline oxides and the crystalline oxides are scattered or in well defined areas, generally concentrated in segregation areas (pores and cracks). The fundamental mineralogical components of the nodules studied are: goethite, lepidocrocite, birnessite, jianshuiite, 10 Å manganates, pyrolusite, quartz and phyllosilicates (illite, smectite, kaolinite). Accessory minerals accompanying these major phases included calcite, dolomite, siderite, rhodochrosite, kutnahorite, pyrite, marcasite, chalcopyrite, potassium feldspar, zircon, rutile, ilmenite, apatite and chlorite. Gypsum is present as a trace secondary mineral.

4.4.1. Iron oxides

Goethite α Fe OOH is an orthorombic Fe-oxide and the dominant phase in all the samples studied occurring with lepidocrocite the dominant minerals in the oxide layers with mean values of 65 wt.%. Goethite presents several types of micro textural features (Figs. 5–8). Goethite has three X-ray reflections, at 4.18 Å, 2.69 Å and 2.45 Å and generally is micro-crystalline to amorphous. SEM observations have revealed abundant structures like-microbes, composed of goethite with a significant quantity of C (up to 24%), filamentous morphology and from 1–3 μm in length (Fig. 8C, arrows). Most of goethite has idiomorphs to subidiomorphs rhombic sections and normally is surrounded by a mixture of phylosilicates, Mn-oxides, and carbonates filling micro-fractures. These crystals are from 2–10 μm in size and normally present internal zones (Figs. 6A, 7A,B, 8A) with goethite concentrated in the external edge. The nucleus of these crystals is formed by a mixture of goethite and Mn-oxides. Goethite normally appears in the oxide layers as rhombic crystals, and less often, forms framboidal and sub-idiomorphic cubic/octahedral aggregates derived from partial or total replacement of pyrite (Figs. 6G, 7B,D). Goethite is also observed substituting carbonates in the bioclastic shells (Fig. 7E). Both rhombohedra crystals and framboidal aggregates appear to be cogenetic (Fig. 7B). Rhombic textures of Fe–Mn oxides are observed within the outer layers affected by the alteration front, although colloform goethite filling the pores has been also frequently observed here (Fig. 7F). Crystalline rhombohedra goethite also appears concentrated in relatively pure layers (laminated structure). Goethite also occurs in rose shaped crystal associations and colloform growths inside cracks within filling of detrital sediments and sparitic carbonates precipitates (calcite and kutnahorite). These “roses” are from 10 to 40 μm in size and are colour zoned internally (Fig. 8B).

4.4.2. Manganese oxides

Birnessite (Na, Ca, K)$_x$ Mn_2O_4*1.5H_2O — jianshuiite (Mg, Mn) Mn_3O_7*3H_2O are monoclinic Mn-oxides with layer structure (7 Å manganates) and the most common manganese oxides present in the layers of the studied nodules, frequently inter-grown with finely crystalline clay minerals and carbonates (Fig. 6A). Birnessite generally is very fine-grained, poorly crystallised, with grey colour and reflectivity, and difficult to recognise optically. The crystallite size

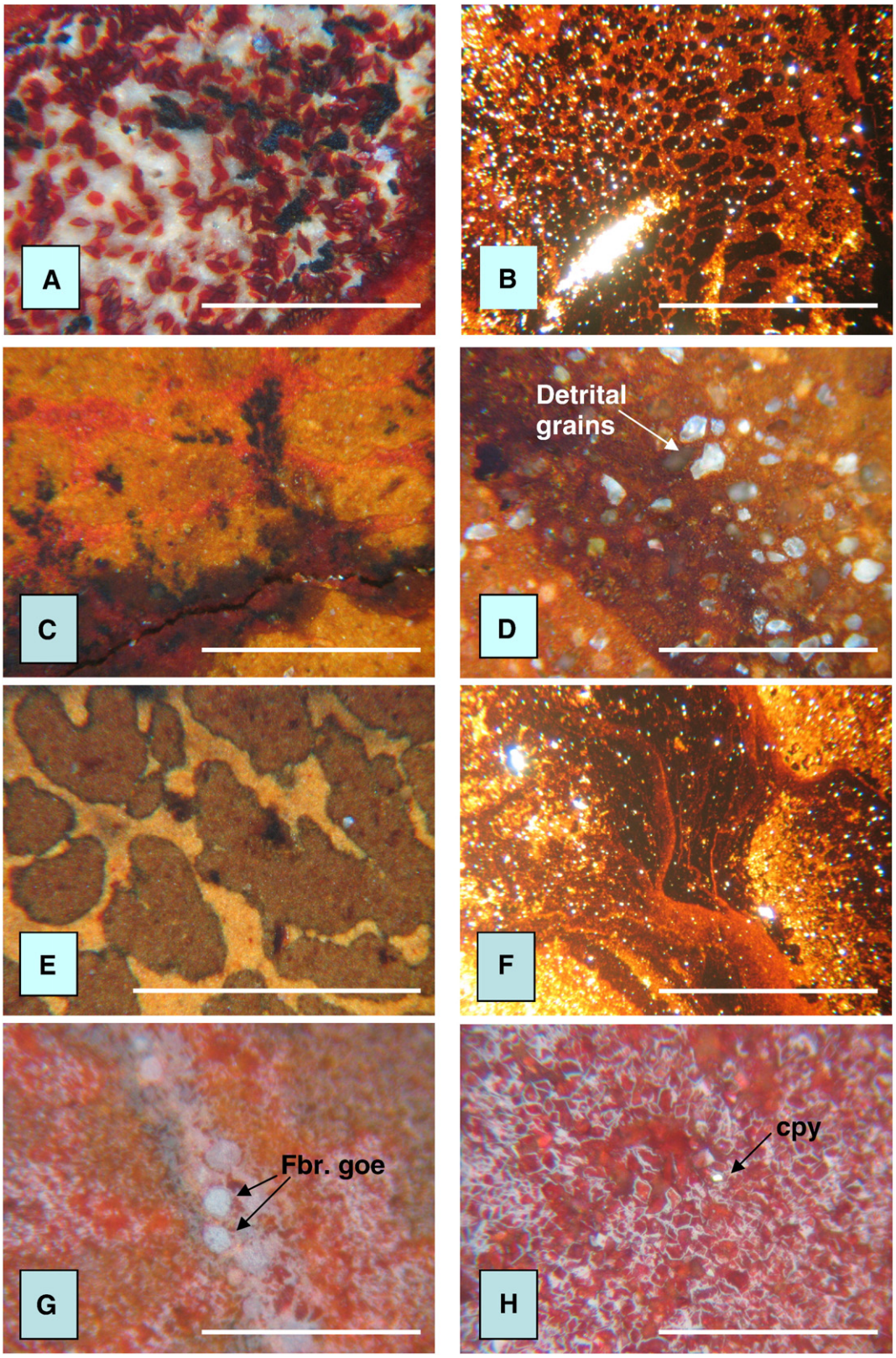

Fig. 6. Photomicrographs in transmitted polarized light. (A) Fe–Mn oxides rhombohedra idiomorphic crystals. (B) Mottled texture developed by the Fe–Mn oxides with abundant scattered detrital silty grains (brightness). (C) Dendritic texture in Mn oxides growing across microfracture (D) Abundant detrital grains with angular edges. (E) Detail of mottled texture with specks rich in goethite and the surrounding material formed by a mixture of Fe–Mn oxides, clay minerals and carbonates. (F) Micro veins filled by iron oxides and calcite. (G) Pseudomorphs of goethite over framboidal pyrites growing in a microfracture (arrows). (H) Rhomboedra Fe–Mn crystals and small grain of authigenic chalcopyrite (arrow). Scale bar represents 1 mm.

must be very small as indicated by the diffuse nature of the X-ray partners obtained. Birnessite has two X-ray reflections, at 7.1 Å, 3.5 Å and 1.41 Å, which vary in sharpness as a result of the crystallite size and manganese content. Mn-oxides have been identified forming part of the rhombohedra goethite zoned crystals, being the nuclei of these crystals formed by very small fibres of Mn oxides. Monomineralic

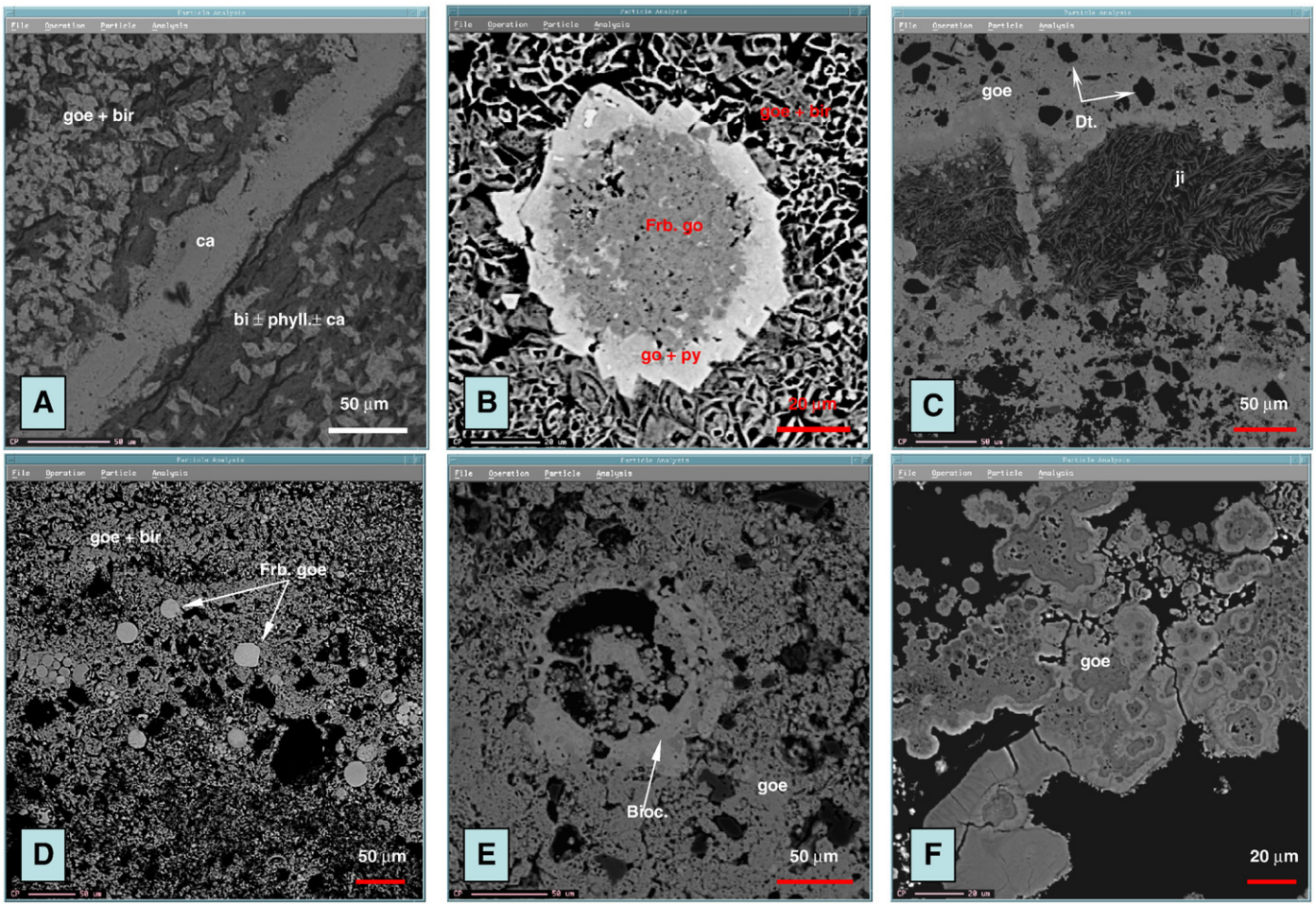

Fig. 7. Mineralogy and internal micro-textures of the nodules, photomicrographs (back-scattered electrons). (A) Oxide layer showing goethite–birnessite rhombic crystals (goe + bir) surrounded by Mn-oxides (bir) and crosscut by a post-accretional crack filled with carbonates (ca). (B) Pyrite aggregate (py) formed by framboids (inside) and idiomorphic cubic crystals (outside), partially pseudomorphised by goethite, paragenetic with Fe–Mn rhombic crystals (goe + bir). (C) Jianshuite (ji) in feather structure filling up a hollow next to micro-crystalline goethite (go) with scattered detrital grains. (D and E) Framboidal goethite (Frb. goe) dispersed or forming aggregates. This goethite is pseudomorphising previous pyrite and bioclast (Bioc.). (F) Colloform goethite filling a post-depositional crack.

specimens are very rare and they are found filling open cavities with spectacular idiomorph, slightly curved acicular crystals (feather structures) (Fig. 7C). SEM observations in natural surfaces, cavities and fresh fractures revealed well-formed crystals not otherwise visible. Probably a mixture of birnessite and jianshuiite are intimately intergrown forming partially oriented intergrowths of platy or fibrous crystals. Manganese oxides represent a mean value of 10 wt.% of the total nodular mass components. Fibrous textures like-microbes coated by Mn-oxides and rich in organic carbon have been identified in pores of some samples (Fig. 9C, arrows).

4.4.3. Carbonates

Carbonate minerals are present in the nodules studied. Nuclei of nodules generally are composed of marl clasts formed essentially by well defined rhombohedra crystals (2–10 µm) of a carbonate between siderite and rhodochrosite partially modified (37.6%FeO, 8.6%MnO) where Fe^{2+} and Mn^{2+}can be substituted by $Ca^{2+}$and Mg^{2+} as reflected in the chemical analyses. EPMA observations allowed the identification of microbial induced fabric in the rhombohedra crystals of these carbonates, where a rounded hollow is frequent in the core of every crystal, probably originally occupied by the micro-organism (Fig. 9A). Calcite and dolomite appear in subangular to angular grains with quartz in detrital rich layers (Fig. 6D). Calcite also occurs in two additional ways; filling secondary pores and cracks (microsparitic to sparitic) and disperse or forming very fine layers of micritic aggregates intercalated with the Fe–Mn growth layers (Fig. 6F). Carbonates from the nuclei and layers show orange luminescence in cathodoluminiscence observations evidencing replacements by Fe and Mn in the carbonates phases. Micritic kutnahorite Ca (Mn, Mg, Fe) $(CO_3)_2$ is filling secondary cracks in some nodules.

4.4.4. Sulphides

Fine-grained pyrite and rarely chalcopyrite and marcasite were observed disseminated in the oxide layers or concentrated along fractures in some nodules (Figs. 5–8). Pyrite normally forms in aggregates of cubic, octahedral and pentagon-dodecahedral micro-crystals (<2 µm) forming framboids (<30 µm) and sometimes framboidal aggregates (Figs. 7B, 8D). Pyrite precursors have not been detected but they probably were present in the first stages of sulphides nucleation. Pyrite also occurs as local replacement of carbonates in shell fragments and frequently is partially substituted by goethite (pseudo-morph) (Fig. 7E). Pyrite commonly appears, partial or totally replaced by goethite, disperses into the Fe–Mn layers and in the marl cores where it forms framboids and sub-idiomorphic aggregates (Fig. 7B, D, E). Marcasite appears rarely, associated with fillings of fractures, and develops tabular crystals. SEM observations revealed secondary gypsum growing over pyrite crystals. Sulphide precipitates imply temporal or spatial changes in the environmental conditions.

4.4.5. Silicates and other

Detrital grains of different minerals, essentially silicates, are present in variable proportion in the nodules. They appear as continuous layers,

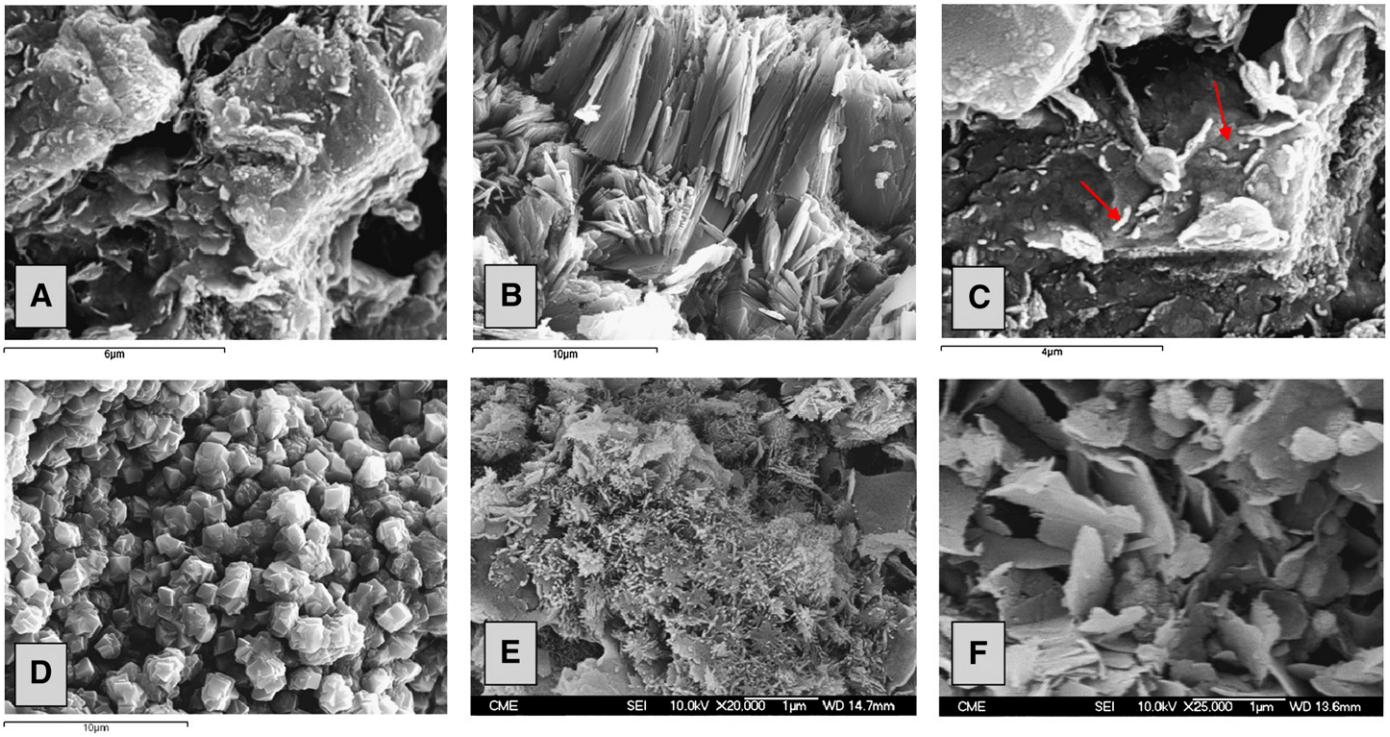

Fig. 8. 3D scanning electron microscope (SEM) micrographs of textural features from the nodular mineralogical components. (A) Rhombohedra crystal of Fe-dolomite pseudomorphised by Fe–Mn oxides. (B) Platy goethite filling micro fractures. (C) Rod-shaped bacteria-like (arrows) coated with a fine grained Fe–Mn oxides precipitate. (D) Pyrite aggregate composed of multiple cubic micro-crystals partially transformed into Fe-oxides. (E) Growth of Fe-oxides in flower shape within the oxide layers. (F) Tabular crystals of Fe–Mn oxides.

dispersed or filling interstices of opaque minerals aggregates. We can identify large angular grains (silt size) of quartz, potassium feldspar, chlorite, calcite, kutnahorite and dolomite, and very round grains of apatite, rutile and zircon. Finely crystalline phylosilicates (illite, smectite, kaolinite, and chlorite) are present as essential minerals (mean values of 12 wt.%) but in minor proportion to the Fe–Mn oxides. Shell fragments of bivalves, gastropods, ostracoda, foraminifera and other benthic organisms, composed of goethite (pseudomorph of pyrite) are present as dispersed and concentrated in detrital-rich layers (Fig. 7E). Quartz, phylosilicates, calcite and dolomite are the most abundant detrital minerals. All these clastic grains have sizes from clay to silt. Zoned grains of carbonates are frequent. We have interpreted these as detrital and the result of the expulsion of fluid and mud through fluid venting structures and/or hemipelagic or contourite sediments. SEM observations have revealed the presence of filosilicate aggregates of well defined crystals in some areas of the nodules which suggests an authigenic origin for part of these minerals.

We can conclude that Fe–Mn oxides and oxihydroxides represent a mean value of 75 wt.% of the nodular mass and they are essentially forming part of the layers. Nuclei are composed of carbonates (siderite and rhodochrosite), silicates in minor proportion and disseminated pyrite as an accessory. Silicates and carbonates disperse in the oxide layers (especially in detrital layers) and are concentrated within the nuclei representing about the 25 wt.% of the nodular mass. The authigenic minerals are goethite, lepidocrocite, pyrite, chalcopyrite, birnessite, jianshuiite, 10 Å manganates, pyrolusite, micritic calcite, dolomite, siderite, rhodochrosite and kutnohorite. Iron oxides also appear as chemical precipitates (hydrogenous oxides), especially in the layers affected by the alteration front.

4.5. Geochemistry

4.5.1. Bulk sample geochemistry

Fe is the most abundant element in the nodules followed by the Mn, Si and Ca. Major, trace and REE element abundances and ratios are presented in the Table 1. The bulk chemical composition of Fe–Mn nodules in the Gulf of Cadiz varies from 0.07 to 0.25 for Mn/Fe ratio. Combined Cu + Ni + Co concentrations are very low, ranging from 0.01% to 0.05% with an average of 0.02%, which is very poor with respect to the mean values for oceanic nodules (0.14%) (Baturin, 1988). Si/Al ratio varies from 1.91 to 3.46, with a mean of 2.52, and is generally below 3 (which is the marine sediment ratio) suggesting the presence of important quantities of clay minerals in the nodules, which is confirmed by the bulk DRX analyses. The greatest standard deviations (61–138) are found for Ni, As, Sr, V and Ba contents. Relative to average crustal abundance (Evans, 1980), several elements are enriched in the nodules from the Gulf of Cadiz by different order factors: As (88), Mn (63), Mo (31), Fe (8), Co (4), V (2) and P (2). Al, Si, K and Na are depleted elements with respect to the crustal mean composition by a factor of between 6 and 11. Fe, Mn, Mo, Co, Ni, As and V are enriched in nodules with respect to the mud breccia associated sediments. Nodules have similar enrichment in elements Mn, Fe, Co or Ni, independent of their sizes. Only Ca shows a relative positive correlation with the sample size, and large nodules are more enriched in Ca than smaller nodules.

Bulk average contents in REE in Fe–Mn nodules (78 µg/g) are lower than in mud breccia associated sediment (198 µg/g). Shale-normalized REE generally show a zero to slightly negative Ce anomaly ranging between −0.11 and +0.04, and positive Eu anomalies. The method used here to describe the values of the Ce anomalies is the logarithm of the ratio of the shale-normalized Ce content to the value obtained by interpolation between shale-normalized La and Nd. La_n/Lu_n are ranging from 0.21 to 0.39 with a mean of 0.29, which means there is a slight fractionation between LREE and HREE. Therefore their REEs concentrations can be explained by significant terrigenous components and by the Mn oxides precipitates.

In bulk samples, iron displays positive correlations with P ($r = 0.41$, $n = 35$), suggesting that it exists as anionic compounds adsorbed in the Fe oxyhydroxides surfaces with positive charges; and Cu ($r = 0.41$, $n = 34$) probably in substitution of Fe cations in goethite. Iron has a negative correlation with Mn ($r = -0.56$, $n = 35$) and S ($r = -0.51$,

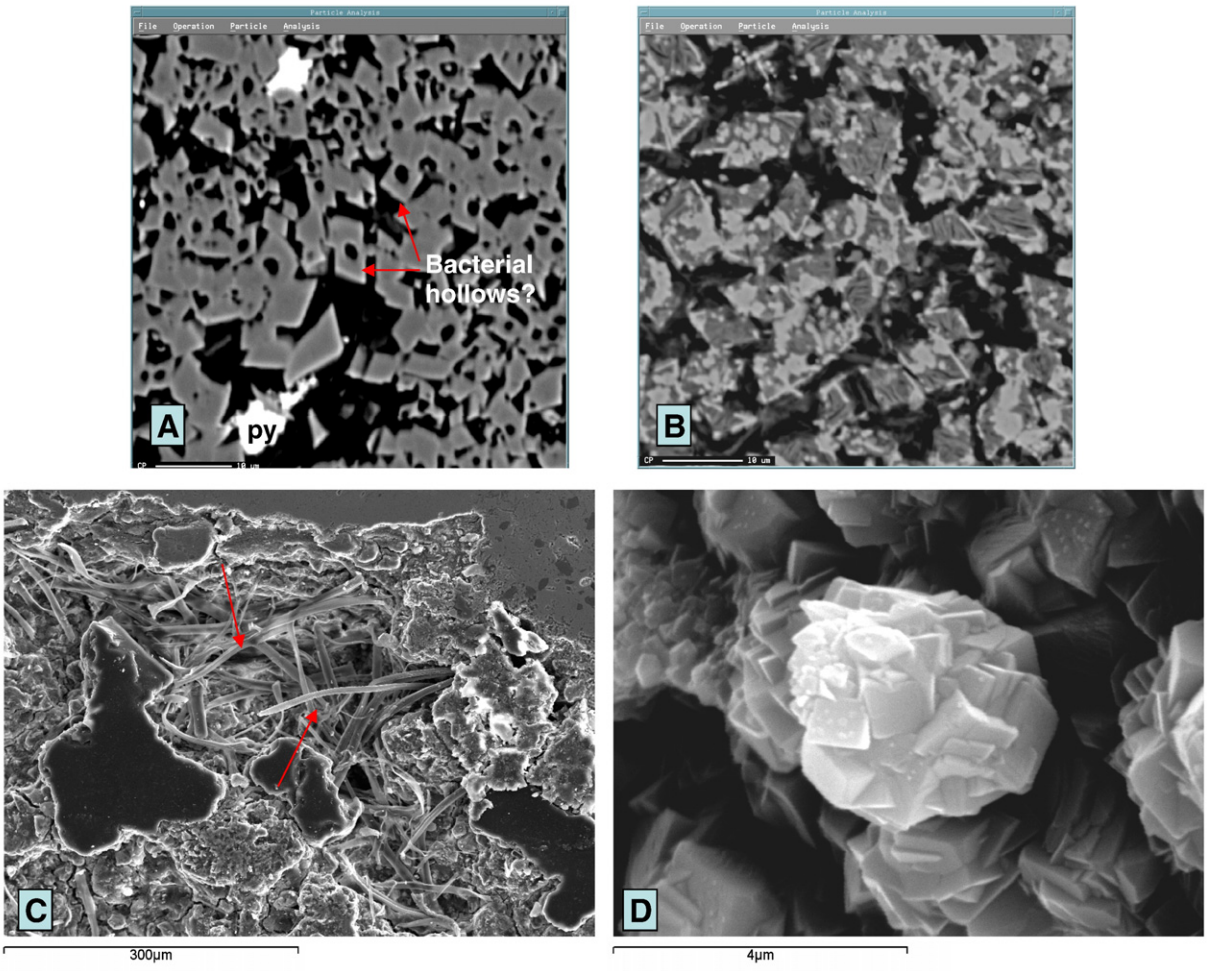

Fig. 9. Organic-derived textures in nodules. (A) Siderite–rhodochrosite microcrystals from the nuclei of one nodule. These rhombohedra crystals frequently show a hollow in their central position (archaea cell?). (B) Rhomboedra crystals of Fe–Mn oxides (pseudomorps of Fe–Mn carbonates) formed by fibrous crystals of Mn oxides in the inner part and Fe oxides in the external edges (layers of the nodule). (C) Fibrous crystals like-microbes coated by Mn oxides in a pore in the external layers of one nodule. (D) Pyrite aggregate formed by multiple cubic crystals sulphate-reducing bacteria derived within the nodule.

$n=24$). Manganese has a strong negative correlation with P ($r=-0.70$, $n=35$), Co ($r=-0.64$, $n=34$), Zn ($r=-0.53$, $n=34$) and positive with Ba ($r=0.62$, $n=34$), Sr ($r=0.42$, $n=34$) and Na ($r=0.36$, $n=35$), is probably linked to birnessite. Ca is correlated with Mg ($r=0.53$, $n=35$) and P ($r=0.50$, $n=35$). High correlations in the group of Si, Al, Ti, K exist between each other, in relation to aluminosilicates. Th and U concentrations present positive correlations ($r=0.48$, $n=34$).

EPMA profiles with analysis points every 50 µm of different elements (Fe, Mn, Co, Ni, Cu, Zn, Si, Al, V, P, As, Ca, and Mg) have been carried out from the nucleus to the outer layers of the different type of nodules. For example, the R1-EPMA profile of the sample ANAS01/D19-01, shows that the external layers affected by the alteration front are strongly enriched in Fe (av. 45%), P (av. 0.29%), Zn (av. 0.08%), V, As, and Co (av. 0.06%) and depleted in Mn (av. 1%) in relation to the rest of the nodule. Pearson correlation coefficients of this profile show a positive correlation of iron (at 99% confidence level) with Co ($n=150$; $r=0.80$), P ($n=150$; $r=0.74$), and V ($n=150$; $r=0.68$) and somewhat lower with As ($n=150$; $r=0.43$). Otherwise, iron has a negative correlation with Ca ($n=150, r=-0.59$) and Mn ($n=150, r=-0.57$). At the same time, Mn has a slight correlation with Mg ($n=150$; $r=0.36$). In bulk samples, Si and Al have a good correlation with each other ($n=25$; $r=0.87$) and with K ($n=25$; $r=0.88$ to 0.92), all present in silicates.

Based on the Pearson correlation matrix for bulk samples, it is possible to divide the elements into four groups defined by similar behaviour: iron, manganese, aluminium and calcium group. The iron group includes P, As, V, Cu, Co and Zn; the manganese group includes Na, Sr, Ba, I, Mo, Li and REE; the aluminium group (detrital aluminosilicate source) is formed by Si, K, Ti, Cr, Rb, Nb, Zr, Sc, I, Li, Y and REE and the calcium group includes Mg, P, B, Co, Ni, As, Zn and Pb. Sulphur participates as S^{2-} and SO_4^{2-} respectively into two groups, an iron group related to remains of sulphides, and a Mn group probably related to traces of authigenic barite and celestine intergrown with Mn-oxides. Cations of Mo, Ba and Sr can be included in the Mn-oxyhydroxides structures.

4.5.2. Composition of mineral phases, individual layers and nuclei

The mean of poorly crystalline Fe–Mn oxides in microprobe analyses are shown in Table 2. EPMA mapping of different associations between iron and Mn oxyhydroxides, and sulphides were obtained. As is frequent in the case of analyses with electron microprobe of Fe–Mn nodules, the element totals were less than 100%. This possibly is the result of incomplete elemental analysis (e.g. H_2O, CO_2, organic matter), difficulty in obtaining smooth polished sections, and the oxide matrix is very porous at microscopic level. The behaviour of trace elements is conditioned by their links with major components present in the nodules.

Goethite concentrates the major contents in Fe and important quantities of S, Co and P. Most pure goethites frequently are pseudomorphic replacements over previous pyrite aggregates or framboids and show highest contents in Fe, S and Pb. If the oxidation process is in the first stages, the goethite also has important contents of Mo.

Table 1
Average content and ratios of major (wt.%), trace and REE elements (μg/g) of the nodules of the Gulf of Cadiz.

Element	Max	Min	Mean	No. of samples analysed	Mud-breccia host sediment
Al (Wt%)	1.98	0.92	1.38	36	6.24
Si	5.26	1.75	3.48	36	22.08
P	0.30	0.05	0.19	36	0.53
K	0.64	0.20	0.34	36	1.56
Na	0.69	0.03	0.26	36	0.11
Ca	6.57	0.62	3.15	36	9.82
Mg	2.21	1.03	1.83	36	1.61
Ti	0.14	0.06	0.10	36	0.37
Fe	45.06	33.06	38.58	36	3.47
Mn	9.12	3.01	6.03	36	0.03
S	0.47	0.05	0.12	24	0.45
LOI	23.24	13.86	18.05	24	15.63
Mn/Fe	0.25	0.07	0.16	36	0.01
Si/Al	3.46	1.91	2.52	36	3.54
Sc (μg/g)	23	13	18	34	25
V	581	147	339	34	118
Cr	62	21	34	34	107
Co	116	60	90	34	8
Ni	404	43	108	34	36
Cu	62	10	39	34	26
Zn	111	32	62	34	59
As	419	23	159	34	11
Br	17	3	10	34	29
Rb	27	11	17	34	76
Sr	601	137	282	34	357
Zr	80	38	63	34	154
Nb	7	3	5	34	12
Mo	69	27	47	34	2
I	50	4	22	34	<d/l (4)
Ba	694	127	352	34	492
Pb	121	6	18	34	14
Bi	1	<d/l (1)	<d/l	34	2
Au	47	<d/l (0.01)	<d/l	10	–
Li	41	7	17	10	–
B	330	167	278	10	–
Th	7	2	4	34	9
U	9	1	4	34	3
∑ REE	99	55	78	24	198
LREE	86	48	68	24	182
HREE	14	6	10	24	15

–: Without data. < d/l: less than detection limit.

Mn-oxyhydroxides, frequently intergrown with goethite, have the major concentrations in Mn and high Fe, Mg, Na, Ca and Ti contents. Also Al and Si are abundant in the areas rich in Mn-oxyhydroxides (mottled structure), which is probably related to the fine mixture between Mn-oxides and clay minerals in these areas. Also these areas are rich in Mg and Ca, which is related to the scattered carbonates present. High contents in Ni and Zn have been located in very pure acicular crystals of secondary Mn-oxyhydroxides growing in open pores. Co, Ni and Zn do not form individual minerals, and they are incorporated within the structure of the Fe–Mn minerals, carbonates and sulphides, that contain a wide spectrum of trace metals. EPMA spot analyses show that goethite has very low Mn/Fe ratios (0.01–0.02) and high Co contents whereas Mn-oxyhydroxides has higher Mn/Fe ratios (5.8) and low Co concentrations (Table 2).

Pyrite is rich in Mo and Pb, and Co and Ni are present in minor quantities. Cu is present especially in chalcopyrite and in minor quantities in goethite and detrital minerals. Gold is below detection limit (0.1 μg/g) in all the samples analysed except one sample with 47 μg/g, where there was a detrital particle of gold mixed with other detrital minerals. Analyses of samples using a scanning electron microscope have not identified Au disseminated or inside of the mineral phases.

Detrital layers which contain a large proportion of terrigenous and biogenic material have high concentrations of terrigenous (Si, Al, Ti, K, Cr, Zr, Y) and biogenic (Ca, Mg) elements. Probably Zr is the best indicator of terrigenous contribution, which increases simultaneously with the major content in detrital minerals in the nodules or in their layers.

The geochemical characteristics of each nodule usually vary from its outer part to the core and from one concentric layer to another. The Mn and Fe concentration curves in EPMA profiles have an irregular shape with different peaks of maximum contents of these metals. The concentric growth pattern of alternating iron and manganese rich layers in the nodules from the Gulf of Cadiz can be attributed to cycling variations in bottom water and pore sediment water conditions. Generally Mn is concentrated close to the nucleus of the nodule, and its concentration decreases towards the periphery. The Fe components show an opposite trend and are more concentrated towards the exterior of the nodule.

The elemental maps obtained using EPMA show the formation of concentric layers of Fe and Mn oxyhydroxides around the nucleus. Nuclei are enriched in Ca, Mg related with carbonates and terrigenous elements (Si, Al) linked to the silicate minerals. Mn enriched layers are associated with the Fe depleted ones. A light positive spatial correlation of Al with Mn and strong between Fe and Co is observed, especially in the mottled texture, where the specks are composed of goethite and the surrounding material are a mixture of Mn-oxides, carbonates and phylosilicates. Dendritic structure is enriched in Mn and Na, and V has positive spatial correlation with Fe in the most exterior part of the nodule (affected by alteration front).

In conclusion, if we compare the correlation coefficients and geochemical analysis in bulk samples, EPMA profiles and maps and mineral phases, it is possible to divide the element contents in the nodules from the Gulf of Cadiz, in four main groups defined by similar behaviour. P, V, As, S, Co, Zn and Cu exhibit strong sympathetic association with Fe forming part or related to Fe-oxyhydroxides or sulphides appearing to concentrate in the laminated structure and the layers affected by the alteration front. Mg, Ca, Na, Sr and Ba are mutually coherent with Mn as part or related to Mn-oxyhydroxides, and concentrated in the inner part of the nodules and the mottled to dendritic textures. Mg, Ca, P, As, V, B, Co, Ni, Zn and Pb, also have a sympathetic association with carbonates, and probably traces of arsenates, phosphates and vanadates, all present in mottled textures and nuclei. Si, Al, Ti, K, Na, Cr, Zr and Y are related to aluminosilicates and other detrital minerals (e.g. zircon, ilmenite), gathered in the detrital structure and nuclei of the nodules. The bulk chemical composition of these nodules therefore represents the weighted average composition of Mn and Fe oxyhydroxides layers with different input level of detrital elements related to the abundance of detrital layers and nature and size of the nodule cores. Oxyhydroxides and sulphides are the most important trace metal-bearing phases in the nodules studied.

4.6. Stable isotopic analyses

Stable sulphur, carbon and oxygen isotopic analyses from 4 nodules from the GDR field are summarised in Table 3. Carbon and

Table 2
Composition of Fe and Mn oxides by electron microprobe analysis.

Mineral	No. analysis	Mg	Mn	P	Mo	As	Fe	S	V	Al	Co	Pb	Ni	Si	Cu	Ca	Zn	Ti	Total
Mn-ox	13	1.98	32.58	0.04	0.03	0.03	5.57	0.08	0.01	2.46	0.04	0.02	0.26	5.16	0.00	1.28	0.09	0.11	49.30
Fe-ox-1	20	0.87	0.59	0.08	0.03	0.05	54.61	0.21	0.01	0.19	0.07	0.04	0.03	0.94	0.01	0.30	0.03	0.02	58.00
Fe-ox-2	17	1.34	0.79	0.27	0.03	0.05	42.05	0.10	0.06	0.46	0.07	0.02	0.04	1.14	0.00	0.43	0.02	0.02	46.76

Mean values for goethite derived from pyrite oxidation (Fe-ox-1), goethite derived from Fe-carbonate (Fe-ox-2) and Mn-oxides derived from Mn-carbonate (Mn-ox).

Table 3
Isotopic composition for calcite, dolomite and pyrite from the Fe–Mn nodules.

Sample reference	Field	$\delta^{13}C$ (‰ PDB)	$\delta^{18}O$ (‰ PDB)	$\delta^{34}S$ (‰ CDT)	Mineralogy
D19-87	GDR	−9.90	−2.57	–	Calcite
D19-103	GDR	−8.58	−0.44	–	Calcite
D19-138	GDR	−8.76	−0.23	–	Calcite
D19-471	GDR	−8.95	−0.78	–	Calcite
D19-87	GDR	−7.18	2.20	–	Dolomite
D19-103	GDR	−6.60	2.66	–	Dolomite
D19-138	GDR	−6.69	2.47	–	Dolomite
D19-471	GDR	−6.53	2.79	–	Dolomite
D19-13	GDR	–	–	−41.00	Pyrite
D19-471	GDR	–	–	12.40	Pyrite
D19-138	GDR	–	–	−9.50	Pyrite

oxygen isotopic signatures were measured in calcite and dolomite rhomboidal crystals extracted from the nucleus of the nodules. Sulphur isotopes were calculated in pyrites obtained from the Fe–Mn layers. In general, the nuclei of the nodules show low depleted $d^{13}C$ values, ranging from −7 to −10‰ and the $d^{18}O_{PDB}$ varies from −2.6 to +2.8‰. The lowest values of $d^{13}C$ (as low as −10‰) correspond to calcite, and dolomite exhibits the highest $d^{13}C$ (−7‰). This variability is also shown in their $d^{18}O$ values, the lowest value to calcite (from −2.6 to −0.2‰) and the highest to dolomite (from 2.2 to 2.8‰). There are not significant differences between the carbon and oxygen isotopic composition of dolomites and calcites from the different nuclei.

Framboidal pyrite aggregates show moderate to highly negative $d^{34}S_{CDT}$ isotopic values ranging between +13 and −41‰.

4.7. Organic carbon and biomarkers

The mean value for TOC analysed in 14 bulk samples is 1.12% with contents ranging between 0.33 and 3.85%. The presence of biomarkers has been detected based on semi-quantitative analyses, over powdered samples of the oxide layers from 10 nodules and nuclei from two nodules (Table 4). Both nucleus and oxide layers present the same biomarkers (Fig. 10). Gas chromatograms (fragmentation ion $m/z=57$) of the total hydrocarbon fraction show similar patterns in all the studied samples, comprising a modal n-alkane distribution with a first concentration maximum at n-C_{18} and an important presence at n-C_{16} and n-C_{20}. Pristane and phytane and/or crocetane (2, 6, 11, 15-tetrametilhexadecano) are present in all the samples analysed. The chromatograms show a convex morphology known as unresolved complex mixture (UCM), characteristic of samples which have undergone an intense degree of marine microbial degradation. The lack of n-alkanes with large chains (>n-C_{25}) suggests absence or low input of terrestrial organic matter, or their intense degradation by bacterial activity. Moreover, the carbon preference index (CPI) ranges from 0.66 to 1.15, which is also characteristic of mature samples. In addition, phenanthrene was detected in all the nodules analysed (fragmentation ion $m/z=178$). This substance is not biological in origin and only occurs in petroleum and coals with a high degree of maturity. Fatty acids are detected in all the nodule samples being composed of saturated acids (C_{14}–C_{18}) which indicates a bacterial origin. Organic sulphur has been detected in the nucleus of one of the two nodules analysed, indicating sulphate-reducing bacterial activity. Esqualene is present in nuclei and oxide layers and it is a lipid present in archaea. Hop-17(21)-ene hopane has not been determined in the oxide layers or nuclei of the nodules.

Three carbonate chimneys from the Vernadsky Ridge (Moroccan Margin) and six chimneys from the Guadalquivir Diapiric Ridge (Iberian Margin) were also studied for biomarkers in order to establish a comparison with the Fe–Mn nodules. All the carbonate chimneys studied show biomarker patterns very similar to the Fe–Mn nodules, also with the presence of phenantrene. Esqualene is present in all the studied chimneys, and hop-17(21)-ene hopane only in two carbonate chimneys from both areas, GDR and VR. PME (2, 6, 10, 15, 19-pentamethylicosane) and esqualane (S, 2, 6, 10, 15, 19, 23-hexametil-tetracosano) have not been identified in the studied chimneys and nodules. This might be due to the small quantity of sample processed (<20 g), where these biomarkers require a large sample to have chemical concentrations sufficient to be detected by chromatography.

4.8. Nodule growth rates

The average growth rate obtained for the studied nodules using the equation proposed by Manheim and Lane-Bostwick (1988) is 2500 mm Myr^{-1} with low and high values ranging between 1400 and 5000 mm Myr^{-1}. Hence, assuming that growth and accretion rate are constant, the minimum age of the nodules varies between 5000 to 30,000 years, depending on the maximum diameter of the oxide layers. Small and big samples exhibit similar growth rates. The

Table 4
Contents of free extractable hydrocarbons in nodule layers.

Sample number	06/253-01	06/253-01	06/253-03	06/253-04	06/253-05	06/253-06	06/253-07	06/253-08	06/253-09	06/253-10
Pristane[a]	3339580	8429274	28590224	19376985	13158767	13085265	3058098	18260724	15979195	13572663
Phytane/crocetane[a]	3918246	7544769	33626743	16503847	11219972	11784885	2919888	16309346	14238969	13389390
C14	0.000	0.369	0.068	0.214	0.111	0.089	0.000	0.035	0.330	0.261
C15	0.059	0.976	0.375	0.693	0.628	0.353	0.013	0.128	0.746	0.697
C16	0.182	1.986	1.049	1.686	1.896	1.043	0.065	0.352	1.589	1.737
C17	0.173	2.309	1.486	1.809	2.135	1.308	0.100	0.409	1.795	2.188
C18	0.271	2.789	1.758	1.923	2.298	1.422	0.119	0.482	2.076	2.628
C19	0.184	2.041	1.577	1.298	1.347	0.826	0.074	0.266	1.459	1.554
C20	0.201	2.259	1.626	1.436	1.628	1.032	0.076	0.278	1.725	1.497
C21	0.153	1.572	1.291	0.938	0.983	0.827	0.047	0.129	1.259	0.934
C22	0.281	1.567	1.092	0.885	0.884	1.012	0.052	0.138	1.271	0.917
C23	0.408	0.979	0.788	0.729	0.410	0.889	0.031	0.058	0.880	0.728
C24	0.411	0.853	0.589	0.481	0.484	0.832	0.045	0.083	0.843	0.664
C25	0.334	0.416	0.490	0.542	0.311	0.667	0.019	0.046	0.525	0.386
C26	0.170	0.441	0.301	0.340	0.305	0.442	0.024	0.075	0.352	0.366
C27	0.085	0.310	0.208	0.124	0.297	0.298	0.016	0.029	0.195	0.178
C28	0.085	0.403	0.131	0.256	0.335	0.264	0.026	0.070	0.281	0.312
C29	0.000	0.000	0.082	0.188	0.229	0.194	0.017	0.027	0.244	0.202
C30	0.000	0.000	0.000	0.144	0.143	0.081	0.010	0.026	0.213	0.112
C31	0.000	0.000	0.000	0.157	0.000	0.124	0.012	0.024	0.248	0.000
Predominant chain	24	18	18	18	18	18	18	18	18	18
Total weight (mg)	2.9965	19.2694	12.9105	13.8435	14.4237	11.7039	0.7464	2.6574	16.0314	15.3583
CPI	0.94	0.72	1.15	1.13	0.82	1.07	0.77	0.61	0.98	0.78

[a] Pristane and phytane/crocetane abundances are given in relative area occupied by their chromatographic peaks.

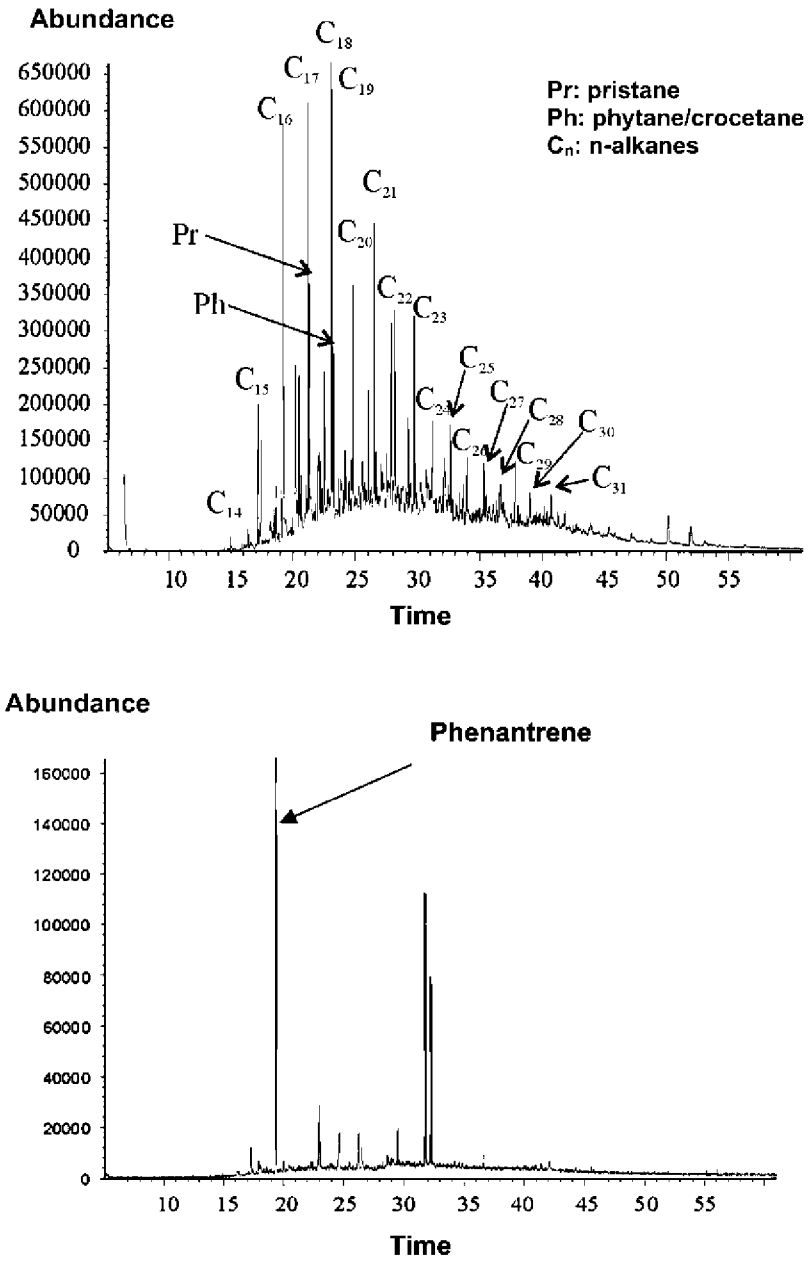

Fig. 10. Organic geochemistry of bitumen's content within the nodular oxide layers. Gas chromatography with mass spectrometer detector (GC-MS). Chromatogram of hydrocarbons extract shows occurrence of homologous series of normal alkanes (n-Cxx). Presence of unresolved complex mixture (UCM) and high concentrations of Pr and Ph suggests influence from biodegradation. The presence of aromatic hydrocarbons as phenanthrene, characteristic of mature petroleum seem be related to migration from deep-seated reservoirs.

growth rate has strong negative correlation with Co ($r=-0.96$, $n=34$), P ($r=-0.75$, $n=35$) and As ($r=-0.71$, $n=34$) and positive with Mn ($r=0.76$, $n=35$).

5. Discussion

In this section, we first compare the results from the studied nodules with other deep-seabed polymetallic nodules, shallow-water and continental margin nodules from other ocean basins and tectonic settings of the world. Secondly, we deal with their specific relationship with hydrocarbon seeps and biomineralization products such as hydrocarbon-derived carbonate chimneys and crusts, and especially with the microbial-mediated activity. Finally, based on the growth rates, mineralogical, textural, and geochemical features, we discuss the genetic model of nodule growth as results of both diagenetic and hydrogenous processes.

5.1. The nodules from the Gulf of Cadiz with respect to polymetallic deep sea and shallow water nodules

With regard to shape, the nodules collected in the Gulf of Cadiz show a wide range of size, with a predominantly tabular morphology (Fig. 4). These tabular or discoidal shapes have been mostly described from shallow-waters nodules like those reported from Kara and Baltic seas (Bogdanov et al., 1995; Glasby et al., 1997). Otherwise, cylindrical nodules are similar to tubular concretions formed around burrows reported in the Black Sea (Baturin et al., 2002). The supply of the different types of nucleus (soft sediment and hard clasts) may be related to the mud breccia flows. Stiff clasts and mud from the mud-breccia flows could act as nucleation sites for the nodules in the areas dominated by extrusions from the mounds. The nodule shape could be related to the shape of the nodule core. Tabular nodules generally have a tabular nucleus and cylindrical nodules are grown around burrow tubes from seafloor sediment horizons.

Physical characteristics such as maximum diameter, density, weight, and porosity are similar to those nodules reported from the Pacific and East Indian Ocean basins (e.g., Raab and Meylan, 1977; Von Stackelberg, 1997; Palma and Pessanha, 2000) and from shallow-waters and continental margin in the Baltic Sea, Gulf of Finland, northern Russian seas and the Black Sea (e.g., Calvert and Price, 1977; Hlawatsch et al., 2002).

Compared to the geochemical average values reported from deep-sea nodules (Baturin, 1988), the studied nodules have high Fe/Mn ratios >1, low trace metals and are enriched in Ca, Mg, Fe, C_{org} and As, although they are quite similar to those reported from Black Sea nodules (Baturin et al., 2002). Numerous authors have classified the oceanic nodules based on the ternary diagram Mn–Fe–(Cu + Ni + Co) × 10. According to this classification, nodules can be diagenetic when the ratio of Mn/Fe>2.5 rich in Cu and Ni and poor in Co; hydrogenetic when Mn/Fe≅1 and relatively high concentrations of Cu + Ni + Co exist, and hydrothermal where Mn/Fe is either very high or very low and normally have low Cu + Ni + Co (Bonatti et al., 1972; Lyle, 1981; Dymond et al., 1984; Fitzgerald and Gillis, 2006). The nodules studied in this work present Mn/Fe <0.25 and low contents of Co, Ni, Cu and REEs in all samples (Table 1). There are abundant references to nodules from shallow waters and continental margins where Fe, Mn and trace metals contents are rather similar to the nodules from the Gulf of Cadiz (Calvert and Price, 1977; Boström et al., 1982; Ingri, 1985; Glasby et al., 1987, 1997; Baturin et al., 2002). All of them display very low Mn/Fe ratios as a result of their growing by combined diagenetic-hydrogenous processes. In addition, the contents in some elements in the nodules from the Gulf of Cadiz (V, As, Ca, Mg, Ni, Co and Mo) are more similar to those obtained in the shallow-water nodules from the Baltic or Black seas (e.g., Volkov, 1979) than to those in the deep-sea nodules. In this sense, the average growth rate of the studied nodules of 2500 mm Myr^{-1} is slower than those calculated for the Baltic Sea nodules with average rates of 20,000 mm Myr^{-1} (Zhamoida et al., 1996; Hlawatsch et al., 2002), but several orders of magnitude higher than growth rates frequently found in hydrogenous deep-sea nodules and crusts (av. 1–6 mm Myr^{-1}) (Hein, 2004). Therefore, fast growth rates emphasize the importance of sediment diagenetic processes (Reyss et al., 1982). Furthermore, this relatively rapid accretion is probably one of the main causes for the overall low content of transition metals in these continental margin nodules. The positive correlation coefficient between Mn and Na, Ca, Mg, Ba and Sr in bulk samples and/or individual layers may be attributed to the stabilization of the birnessite–jianshuite structures by monovalent and divalent cations as numerous researchers describe in other works (Burns and Burns, 1977; Bischcoff et al., 1981). As in the other oceanic manganese deposits (e.g., Burns and Burns, 1979), the mineralogy of the Fe–Mn oxides in the studied nodules has been considered to be the main seat for heavy metals.

5.2. Relationships between Fe–Mn nodules, hydrocarbon seeps, bacterial activity and methane-derived precipitates

The main distinctive characteristic of studied nodules with regards to other reported Fe–Mn nodules fields is their association with hydrocarbon-derived carbonate chimneys and crusts which were photographed and recovered near the studied nodules. Manganese nodule fields extend across large surfaces, probably related to areas of discharge of fluids from faults systems in the flanks and base of extrusive edifices from the Guadalquivir Diapiric Ridge (Fig. 2). Topographic highs such as Guadalquivir Diapiric Ridge may act as sites for crustal fluid discharge and the consequent accumulation of mineral deposits and development of vent-associated faunal communities. Numerous authors have reported these phenomenon's in other oceanic areas in the world (Alt, 1988; Mottl et al., 1998). Mud volcanoes and diapiric ridges present large heat flow and geochemical anomalies with respect to the surrounding area and are related to fault structures (Gardner, 2001). These structures facilitate fluid flow between deep crustal materials and the ocean floor. Mud volcanoes and diapiric ridges are the expression of these crustal fluid discharge sites, and probably act as recharge sites for seawater. Besides this physical association, several other evidences support the close relationship between the studied nodules and hydrocarbons seeps. The organic carbon contained in the studied samples (av. 1.12%) is substantially higher than in deep-sea polymetallic nodules (av. 0.1%; Baturin, 1986) but quite similar to ferromanganese concretions from the Black Sea (av. 0.7%; Baturin et al., 2002). Furthermore, the oxide layers of the studied nodules contain mature hydrocarbons derived from bacterial activity, with the presence of aromatic hydrocarbons as phenanthrene, characteristic of mature petroleum. These hydrocarbons also have been found within the methane-derived carbonate chimneys and crusts from the area (González, 2008). In addition, mature hydrocarbon gases (Ro<1.2%) derived from kerogen type II and a mixture of kerogens of types II and III have been reported from sediments in the Moroccan mud volcano province of the Gulf of Cadiz (Stadnitskaia et al., 2006). Carbonate formation induced by anaerobic oxidation of methane (AOM) is confined in oxidising sea-waters, to anoxic sediment layers that are later exposed by erosional processes (e.g. Jørgensen, 1989; Stakes et al., 1999; Peckmann et al., 2001). Therefore, the present position of the carbonate chimneys and crusts, lying on the seafloor, seems to point to exhumation by bottom current activity of the Mediterranean outflow waters. SEM observations in carbonate minerals (siderite–rhodochrosite) from the nuclei of Fe–Mn nodules, with well developed idiomorphic to sub-idiomorphic rhombohedra crystals (Fig. 9A), and $d^{13}C$ low values (as low as −10‰ PDB) can be interpreted as signs of the important involvement of microbial activity in the formation of these authigenic carbonates within the sediment column at the place where the nodules are growing. The carbon isotopic composition of these carbonates can be related to the mixing of different carbon sources: biogenic methane, thermogenic methane, fermentation of organic matter, dissolved carbonate tests, and seawater. The presence of phenantrene as well as mature hydrocarbons in the studied samples suggests that thermogenic hydrocarbons are the essential contributor to the carbonates generation. The fractionation of the carbon would be conditioned by the oxidation of these hydrocarbons in their reservoirs and migration process across fractures from the reservoirs to the seafloor.

Micro-biological synthesis of oxides, carbonates and sulphides in nodules and sediments has been reported by numerous authors (e.g., Hein and Koski, 1987; Nealson and Myers, 1992; Kohn et al., 1998; Stein et al., 2001). Micro-organisms such as archaeas, sulphate-reducing bacteria (SRB) and sulphide-oxidising bacteria (SOB) have been found in sediments and carbonates from mud volcanoes and mud-carbonate ridges in the Gulf of Cadiz (e.g., Niemann et al., 2006). These organisms use the hydrocarbon-enriched fluids from seeps in their vital activity, giving rise directly or indirectly to minerals: carbonates and sulphides in an anoxic environment (by archaeas and SRB respectively) and oxides in oxidising environment (by SOB). Pyrites from the nodules exhibit textural (clots and framboids) geochemical (abundance of organic sulphur and C_{org}) and isotopic ($d^{34}S_{CDT}$ between +13 and −41‰) typical characteristics of microbial-mediated pyrite, formed by anoxic oxidation of methane through a syntrophic interaction between methanotropic archaea and SRB (Hinrichs and Boetius, 2002). The idiomorphic crystals of Fe–Mn carbonates from the nodular nuclei indicate that recrystallisation processes occurred after the mud extrusion, within the mud flows reducing sediment. These carbonate crystals present a hollow in their central position (Fig. 9A) that probably correspond to the archaea cell cast, also observed in hydrocarbon-derived carbonate chimneys from the area. In this sense, filamentous and bulbous textures observed in Fe–Mn oxides in the nodules (Figs. 8C, 9B,C) could have been generated by SOB within the upper oxidising sediment. Moreover, the existence of low molecular saturated fatty acids (C_{14}–C_{18}), whose

content usually sharply decreases during burial, is indicating recent bacterial participation in the organic matter formation, probably linked with bacterial mineralization processes. Fatty acids present as bacterial markers in Fe–Mn nodules from the Pacific and Indian oceans, are related with the genetic types and element distribution in those deposits (Aleksandrova and Poluyaktov, 1996).

5.3. Genetic model

Mineralogical, textural and geochemical evidence of how these nodules might grow on and beneath seabed sediments by successive diagenetic and hydrogenous processes as a consequence of alternating episodes of burial and exhumation is discussed here. The presence of previous detrital layers and burrows enclosed within the nodules from the Gulf of Cadiz may indicate that they could be formed beneath the sediment–water interface and later exposed by erosion as occurs with carbonate chimneys and crusts. In this area the MOW undercurrent is characterised by current velocities of 20–30 cm/s (Hernández-Molina et al., 2006). Variations in the metal content with respect to the nodule sizes have been observed by numerous authors in different oceanic areas (Von Stackelberg, 2000; Jauhari and Pattan, 2000) which seem to be related to the intervention of various processes to nodular accretion (diagenetic, hydrothermal, hydrogenetic). In the nodules studied in this work we do not observe any apparent correlation between metal content and nodules sizes, therefore size may be due to the dominance of the diagenetic process for nodular accretion in the area studied, being less important then other growth models. According to Von Stackelberg (2000) the dendritic and dense laminated textures observed in our samples are characteristic of diagenetic growth within the sediment.

As reported from other shallow-water concretions (e.g., Loch Fyne, Scotland; British Columbia; Baltic Sea), the nodules recovered from the Gulf of Cadiz are found lying over brown oxidised sediments, whereas its subsurface sediments, below a few millimetres to centimetres, consist of olive-grey reduced muds containing H_2S and sulphides (Somoza et al., 2003). Textural equilibrium observed between rhombohedra oxide crystals and pyrite framboids (partial or totally pseudomorphised by goethite) points out to that both crystalline structures, rhomboidal and framboidal have been formed at the same time and therefore, both are syn-genetic. However, redox conditions necessary for pyrite and oxides formation are radically different. Presently in this area, carbonates and pyrites grow jointly at depths 20–200 cm below sea floor within the sulphate–methane transition zone (SMT) under anaerobic conditions as a consequence of the microbial-mediated methane oxidation and sulphate reduction (Niemann et al., 2006). Our observations suggest that crystals of goethite-Mn oxides are derived from hydrocarbon-derived carbonates (siderite to rhodochrosite) in origin. In this way, the present rhombic oxide crystals represent pseudomorphs of carbonate micritic crystals originated by diagenetic transformations from Fe–Mn carbonates to Fe–Mn oxides under oxidising conditions. Similar textures and primary associations of pyrite-carbonates have been observed both in mud breccia, high-sulphide sediments ejected by fluid venting (Martín-Puertas et al., 2006), and in hydrocarbon-derived carbonate chimneys from the Gulf of Cadiz (e.g., Díaz-del-Río et al., 2003; González et al., 2006b). In addition, goethite replacements of carbonates have been observed in burial corals from mud diapiric ridges in the Gulf of Cadiz (Kozlova et al., 2007). Carbon dioxide produced by the transformation of carbonates to oxides could have generated fluidification discontinuities observed in the oxide layers. As a result of the strong erosive action of the sea-bottom undercurrents, iron-sulphides formed within a highly reduced zone only few centimetres below sediments, and may have come in contact with suboxic to oxic interstitial water from oxidizing oceanic-bottom waters. The exhumation process drives the oxidation of Fe^{2+} and Mn^{2+} to Fe^{3+} and Mn^{3+}, Mn^{4+} thus, to form the Fe–Mn oxyhydroxides. Therefore different factors could control the nodule growth: supply of metals from pore sediments, intensity of diagenetic processes, Eh potential, microbiological activity, and erosive action of bottom currents.

The strong Fe enrichment observed in the studied nodules when compared to deep sea nodules, may be explained as a consequence of being pyrites and Fe-rich carbonates where sediment is the primary source of iron. On the other hand, nodules studied are depleted in Mn in the outer layers that are affected by the alteration front, and probably formed after the exhumation. This fact is explained by the high geochemical mobility of Mn as a response to changes in the environmental conditions. Thus, the chemistry of the MOW in the area, which is characterised by low values of dissolved oxygen in the water (160–170 μmol/kg) (Cabeçadas et al., 2002) could have contributed, together with the intense undercurrent, to the depletion of manganese found in the outer layers in the exhumed nodules. In contrast, these outer layers are iron-rich indicating a recent period of stagnation in the nodule growth. The high porosity observed in these outer layers reflects dissolution processes also related to changes in the geochemistry of the environment. In nodules from the Central Indian Ocean Basin Jauhari and Pattan (2000) found iron and cobalt concentrated close to the nucleus (hydrogenetic in origin), and Mn more concentrated in the exterior layers (early diagenetic). In the nodules studied here we can observe Mn more concentrated in the exterior layers in some samples without a developed alteration front, which could be related to diagenetic post-depositional processes (growing of dendritic structures across fractures) and recent exhumation. Zero to negative Ce anomaly in the studied nodules suggests that they were formed at a lower redox level in the vicinity of the redox boundary, and agree with a diagenetic growth and later exhumation process. The presence of a second generation of sulphides and kutnahorite precipitates that are filling pores and cracks of nodules implies the existence of reduced micro-niches in an oxic environment. Reducing micro-niches with sulphide precipitates have been observed in Fe–Mn nodules (e.g., Baturin, 1986).

Therefore Mn-rich and Mn–Fe mixed layers may represent active growth beneath the sediment–water interface in the vicinity of the redox boundary where Mn and Fe are directly supplied from sediment pore waters. Fe-rich layers are related to periods of exposure to the bottom waters with very low growth rates, iron oxides precipitated from the sea-water and Mn removed from the external part of the nodules. Hence, if the nodules lie uncovered on the sea-floor they grow hydrogenetically whereas they are covered by sediment then they grow diagenetically.

6. Summary and conclusions

Here we report the first discovery and sampling of Fe–Mn nodules in the continental margin of the Gulf of Cadiz. 561 nodules were recovered during the Anastasya-01 cruise (TASYO project). The nodule fields extend along the mid-continental slope at an average depth of 900 m on continental crust in contrast to deep sea nodules, which grow on abyssal plains of oceanic crusts (Cronan, 1977). The most striking point of the nodule field reported here is that the area is characterised by a high abundance of mud volcanoes, diapirs, pockmarks and carbonate chimneys, reflecting a great release of deep-seated hydrocarbons to the sea floor through faults and sediment pores (e.g., Somoza et al., 2002; León et al., 2007). In this sense, nodules were found together with large amounts of hydrocarbon-derived chimneys and crusts and mud breccia deposits at the base of a sequence of carbonate-mud mounds, the Guadalquivir Diapiric Ridge, that acts as a barrier for the Mediterranean outflow bottom current (Díaz-del-Río et al., 2003).

The nodules, fundamentally tabular-irregular in morphology, grow concentrically around a nucleus of Miocene blue marls ejected by fluid venting from the underlying units of the so-called "Olistostrome Mass" (Maldonado et al., 1999). Internally, nodules consist of layers, clearly concentric in small nodules, but forming complex morphologies in large and composite nodules. All nodules studied show similar petrographic

characteristics being mainly formed by Fe–Mn oxyhydroxides. These oxides display characteristic rhombic shapes with a relatively big size of crystals with regard to cryptocrystalline Fe–Mn oxides in comparison to other shallow or deep ocean nodules. Quartz and phyllosilicates (detrital) are commonly present although in much smaller proportion than the Fe–Mn oxyhydroxides. The textures developed by the Fe and Mn oxyhydroxides are dendritic, massive, laminated and mottled to dendritic. Nodules show a quite similar geochemistry to shallow water nodules rather than deep-sea polymetallic nodules. They display high mean abundance of Fe (38.6%), moderate Mn (6.0%), and low contents of trace metals, REEs. Based on the cobalt chronometer method, an average of 2500 mm Myr^{-1} has been calculated for nodule growth, being several magnitudes faster than those from reported deep sea polymetallic nodules.

We propose for nodule genesis both diagenetic and hydrogenous processes, beneath and on seabed sediment, as a consequence of alternating episodes of burial and exhumation due to the bottom current activity of the Mediterranean outflow waters. The presence of mature hydrocarbons such as phenanthrene within the nodules indicates that diagenetic processes are related to deep-seated hydrocarbon seeps, probably through microbial-mediated anaerobic oxidation of hydrocarbons. On the other hand, the variability in the hydrogenous nodule growth may be related to the interface between the oxygenated North Atlantic deep waters and the briny Mediterranean outflow waters.

All these considerations suggest that the formation of these Fe–Mn nodules fields implies new considerations on the importance of role of fluid venting in the Gulf of Cadiz to form complex deep-water chemosynthetic systems composed of distinct types of mineralization process, products, and mineral ores.

Acknowledgements

This work has been funded thanks to a research fellowship of the Geological Survey of Spain within the framework of the European Science Foundation EuroCORE-EuroMARGINS projects: "MOUNDFORCE" (O1-LEC-EMA06F, REN-2002-11668-E-MAR) and "MVSEIS" (O1-LEC-EMA24F, REN-2002-11669-E-MAR). The authors thank all the scientific and technical personnel who participated in the oceanographic cruises of the "TASYO" project, of the R/V "*Cornide de Saavedra*" and R/V "*Hespérides*", for the data acquisition and their expertise in collecting the samples, essential for the elaboration of this paper. We also thank personnel of the "Centro de Microscopía Electrónica Luis Bru", "Universidad Complutense de Madrid" (UCM), "Centro de Astrobiología" (CSIC/INTA), "Laboratorio de Estratigrafía Biomolecular" (UPM), "Servicio General de Isótopos Estables" (USAL) and to the laboratories of the "Instituto Geológico y Minero de España" (IGME), the facilities given for the use of its equipments. The comments and suggestions of Dr. Joan Gardner and two anonymous reviewers considerably helped to improve the manuscript.

References

Al-Aasm, I., Taylor, B.E., South, B., 1990. Stable isotope analysis of multiple carbonate samples using selective acid extraction. Chem. Geol. (Isotope Geosci. Sect.) 80, 119–125.

Aleksandrova, O.A., Poluyaktov, V.F., 1996. Fatty acid composition of the iron–manganese nodules and surrounding sediments in the Pacific and Indian oceans. Oceanology 35 (5), 630–637.

Alt, J.C., 1988. Hydrotermal oxide and nontronite deposits on seamount in the eastern Pacific. Mar. Geol. 81, 227–239.

Auzende, J.M., Olivet, J.L., Pastouret, L., 1981. Implication structurales et paléogeographiques de la presence de Messinien a l'ouest de Gibraltar. Mar. Geol. 43, 9–18.

Baraza, J., Ercilla, G., 1996. Gas-charged sediments and large pockmark like features on the Gulf of Cadiz slope (SW Spain). Mar. Pet. Geol. 13 (2), 253–261.

Baturin, G.N., 1986. Geochemistry of Oceanic Ferromanganese Nodules. Nauka, Moscow. 328 pp.

Baturin, G.N., 1988. The Geochemistry of Manganese and Manganese Nodules in the Ocean. D. Riedel Publ. Co. 342 pp.

Baturin, G.N., Gorshkov, A.I., Magazina, L.O., Bogdanova, O.Yu., 2002. Structure and composition of ferromanganese-phosphate nodules from the Black Sea. Lithol. Min. Resour. 37 (4), 374–385.

Bischcoff, J.C., Piper, D.Z., Leong, K., 1981. The aluminosilicate fraction of North Pacific manganese nodules. Geochim. Cosmochim. Acta 45, 2047–2049.

Bogdanov, Yu.A., Gurvich, E.G., Bogdanova, O.Yu., Ivanov, G.V., Isaeva, A.B., Muravév, K.G., Gorshkov, A.I., Dubinina, G.I., 1995. Ferromanganese nodules of the Kara Sea. Oceanology 34 (5), 722–732.

Bonatti, E., Kraemer, T., Rydell, H., 1972. Classification and genesis of submarine iron–manganese deposits. In: Horn, D.R. (Ed.), Ferromanganese deposits of the ocean floor. Arden House, New York, pp. 149–165.

Bonnin, J., Olivet, J.L., Auzende, J.M., 1975. Structure en nappe a l'ouest de Gibraltar. C. R. Acad. Sci. 280 (5), 559–562.

Borges, J.F., Fitas, A.J.S., Bezzeghoud, M., Teves-Costa, P., 2001. Seismotectonics of Portugal and its adjacent Atlantic area. Tectonophysics 337, 373–387.

Boström, K., Wiborg, L., Ingri, J., 1982. Geochemistry and origin of ferromanganese concretions in the Gulf of Bothnia. Mar. Geol. 50, 1–24.

Burns, V.M., Burns, M.G., 1977. Mineralogy. In: Glasby, G.P. (Ed.), Marine manganese deposits. Elsevier Oceanography Series, vol. 15, pp. 185–248. Amsterdan.

Burns, R.G., Burns, V.M., 1979. Manganese oxides. In: Burns, R.G. (Ed.), Marine Minerals, Reviews in Mineralogy. Min. Soc. Am., vol. 6, pp. 1–46. Washington, D.C.

Cabeçadas, G., Brogueira, M.J., Gonçalves, C., 2002. The chemistry of Mediterranean outflow and its interactions with surrounding waters. Deep Sea Res. Part II 49, 4263–4270.

Calvert, S.E., Price, N.B., 1977. Shallow water, continental margin and lacustrine nodules: distribution and geochemistry. In: Glasby, G.P. (Ed.), Marine manganese deposits. Elsevier Oceanography Series, Amsterdam, pp. 45–86.

Cavazza, W., Roure, M.R., Spakman, W., Stampli, G.M., Zigler, P.A., 2004. The Trasmed Atlas: the Mediterranean Region from Crust to Mantle. Springer-Verlag Berlin Heidelberg, Germany. 141 pp.

Coleman, M.L., Moore, M.P., 1978. Direct reduction of sulfates to sulfur dioxide for isotopic analysis. Anal. Chem. 50 (11), 1594–1595.

Cronan, D.S., 1977. Deep-sea nodules: distribution and geochemistry. In: Glasby, G.P. (Ed.), Marine manganese deposits. Elsevier Oceanography Series, Amsterdam, pp. 11–44.

Dekov, V.M., Savelli, C., 2004. Hydrothermal activity in the SE Tyrrhenian Sea: an overview of 30 years of research. Mar. Geol. 204, 161–185.

Dewey, J.F., Helman, M.L., Turco, E., Hutton, D.H.W., Knott, S.D., 1989. Kinematics of the Western Mediterranean. In: Coward, M., Dietrich, D., Park, R.G. (Eds.), Alpine Tectonics. Alpine Tectonics. Special Publication Geological Society of London, vol. 45. London, pp. 265–283.

Díaz-del-Río, V., Somoza, L., Martínez-Frías, J., Hernández-Molina, F.J., Lunar, R., Fernández-Puga, M.C., Maestro, A., Terrinha, P., Llave, E., García, A., García, A.C., Vázquez, J.T., 2001. Carbonate chimneys in the Gulf of Cadiz: initial report of their petrography and geochemistry. Final Proc. Int. Conf. Geological Processes on Deep-Water European Margins, Moscow, Russia. UNESCO IOC Workshop Report, vol. 175, pp. 53–54.

Díaz-del-Río, V., Somoza, L., Martínez-Frías, J., Mata, M.P., Delgado, A., Hernández- Molina, F.J., Lunar, R., Martín Rubí, J.A., Maestro, A., Fernández-Puga, M.C., León, R., Llave, E., Medialdea, T., Vázquez, J.T., 2003. Vast field of hydrocarbon-derived carbonate chimneys related to the accretionary wedge/olistostrome of the Gulf of Cadiz. Mar. Geol. 195, 177–200.

Dymond, J., Lyle, M., Finney, B., Piper, D.Z., Murphy, K., Conard, R., Pisias, N., 1984. Ferromanganese nodules from MANOP Sites H, S and R-control of mineralogical and chemical composition by multiple accretionary processes. Geochim. Cosmochim. Acta 48, 931–950.

Evans, A.M., 1980. An Introduction to Ore Geology. Blackwell Scientific Publication, Oxford. 356 pp.

Fernández-Puga, M.C., 2004. Diapirismo y estructuras de expulsión de gases hidrocarburos en el talud continental del Golfo de Cádiz. PhD. Thesis. University of Cadiz. 335 pp.

Fitzgerald, C.E., Gillis, K.M., 2006. Hydrothermal manganese oxide deposits from Baby Bare seamount in the Northeast Pacific Ocean. Mar. Geol. 225, 145–156.

Gardner, J.M., 2001. Mud volcanoes revealed and sampled on the Moroccan continental margin. Geophys. Res. Lett. 28 (2), 339–342.

Glasby, G.P. (Ed.), 1977. Marine Manganese Deposits. Elsevier Oceanography Series, vol 15. Amsterdan. 523 pp.

Glasby, G.P., Gwozoz, R., Kunzendorf, H., Friedrich, G., Thijssen, T., 1987. The distribution of rare earth and minor elements in manganese nodules and sediments for the equator and S.W. Pacific. Lithos 20, 97–113.

Glasby, G.P., Emelyanov, E.M., Zhamoida, V.A., Baturin, G.N., Leipe, T., Bahlo, R., Bonacker, P., 1997. Environments of formation of ferromanganese concretions in the Baltic Sea: a critical review. In: Nicholson, K., Hein, J.R., Bühn, B., Dasgupta, S. (Eds.), Manganese Mineralization: Geochemistry and Mineralogy of Terrestrial and Marine Deposits. Special Publication Geological Society of London, vol. 119. London, pp. 213–237.

González, F.J., 2004. Los nódulos de hierro-manganeso del Golfo de Cádiz. Trabajo de Suficiencia Investigadora. Facultad de Ciencias Geológicas. Universidad Complutense de Madrid. 76 pp.

González, F.J., 2008. Nódulos y costras de hierro-manganeso en el Golfo de Cádiz y la Antártida: génesis e implicaciones paleoceanográficas. PhD. Thesis. Complutense University of Madrid. 519 pp.

González, F.J., Somoza, L., Lunar, R., Martínez-Frías, J., Martín Rubí, J.A., Díaz-del-Río, V., 2006a. Nódulos de Fe–Mn: El nuevo descubrimiento del Golfo de Cádiz. Bol. Geol. Min. 117, 491–497.

González, F.J., Pinheiro, L.M., Magalhães, V.H., Ivanov, M., Somoza, L., Merinero, R., 2006b. Sulphate-reducing bacteria as a nucleation sites for pyrite in carbonate chimneys from the Vernadsky Ridge, Moroccan margin of the Gulf of Cadiz. Final Proc. Int. Conf. Geological processes on Deep-Water European Margins, Moscow, Russia. UNESCO IOC Workshop Report n°, vol. 201, pp. 19–22.

González, F.J., Somoza, L., Lunar, R., Martínez-Frías, J., Martín Rubí, J.A., Torres, T., Ortiz, J.E., Díaz-del-Río, V., 2007. Fe–Mn nodules associated with hydrocarbon seeps: a new discovery in the Gulf of Cadiz. Episodes 30 (3), 187–196.

Gutscher, M.-A., Malod, J., Rehault, J.-P., Contrucci, I., Klingelhoefer, F., Mendes-Victor, L., Spakman, W., 2002. Evidence for active subduction beneath Gibraltar. Geology 30, 1071–1074.
Hein, J.R., 2004. Cobalt-rich ferromanganese crusts: global distribution, composition, origin and research activities, in: ISA (Ed,), Minerals other than polymetallic nodules of the International Seabed Area. Workshop Report, Kingston, Jamaica, pp. 188–272.
Hein, J.R., Koski, R.A., 1987. Bacterially mediated diagenetic origin for chert-hosted manganese deposits in the Franciscan Complex, California Coast Ranges. Geology 15 (8), 722–726.
Hein, J.R., Schulz, M.S., Kang, J.K., 1990. Insular and submarine ferromanganese mineralization of the Tonga–Lau region. Mar. Min. 9, 305–354.
Hernández-Molina, F.J., Llave, E., Somoza, L., Fernández-Puga, M.C., Maestro, A., León, R., Medialdea, T., Barnolas, A., García, M., Díaz-del-Río, V., Fernández Salas, L.M., Vázquez, J.T., Lobo, F.J., Alveirinho Díaz, J.A., Rodero, J., Gardner, J., 2003. Looking for clues to paleoceanographic imprints: a diagnostic of the Gulf of Cadiz contourite depositional system. Geology 31 (1), 19–22.
Hernández-Molina, F.J., Llave, E., Stow, D.A.V., García, M., Somoza, L., Vázquez, J.T., Lobo, F.J., Maestro, A., Díaz-del-Río, V., León, R., Medialdea, T., Gardner, J., 2006. The contourite depositional system of the Gulf of Cadiz: a sedimentary model related to the bottom current activity of the Mediterranean outflow water and its interaction with the continental margin. Deep Sea Res. Part II 53, 1420–1463.
Hinrichs, K.-U., Boetius, A., 2002. The anaerobic oxidation of methane: new insights in microbial ecology and biogeochemistry. In: Wefer, G., Billett, D., Hebbeln, D., Jørgensen, B.B., Schlüter, M., van Weering, T.C.E. (Eds.), Ocean Margin Systems. Springer-Verlag, Berlin, pp. 457–477.
Hlawatsch, S., Neumann, T., van den Berg, C.M.G., Kersten, M., Harff, J., Suess, E., 2002. Fast-growing, shallow-water ferro-manganese nodules from the western Baltic Sea: origin and modes of trace element incorporation. Mar. Geol. 182, 373–387.
Ingri, J., 1985. Geochemistry of ferromanganese concretions and associated sediments in the Gulf of Bothnia. PhD thesis, University of Lulea.
ISA, International Seabed Authority, 1999. Deep-seabed polymetallic nodule exploration: development of environmental guidelines. Proceedings of International Seabed Authority's workshop held in Sanya, Hainand Island, People's Republic of China, 1–5 June 1998. 289 pp.
ISA, International Seabed Authority, 2000. Regulation on prospecting and exploration for polymetallic nodules in the area (ISBA/6/A/18). In Selected decisions and documents of the Sixth Session, pp. 31–68.
Ivanov, M.K., Kenyon, N., Nielsen, T., Wheeler, A., Monteiro, J., Gardner, J., Comas, M., Akhmanov, G., Akhmetzhanov, A., Scientific Party of the TTR-9 cruise, 2000. Goals and principle results of the TTR-9 cruise. Final Proc. Int. Conf. Geological processes on European Continental Margins, Granada, Spain. UNESCO IOC Workshop Report, vol. 168, pp. 24–25.
Jauhari, P., Pattan, J.N., 2000. Ferromanganese nodules from the Central Indian Ocean Basin. In: Cronan, D.S. (Ed.), Handbook of marine mineral deposits. CRC Press, pp. 171–195.
Jørgensen, N.O., 1989. Holocene methane-derived, dolomite-cemented sandstone pillars from the Kattergat, Denmark. Mar. Geol. 88, 71–81.
Kohn, M.J., Riciputi, L.R., Stakes, D., Orange, D.L., 1998. Sulphur isotope variability in biogenic pyrite: reflections of heterogeneous bacterial colonisation? Am. Mineral. 83, 1454–1468.
Kozlova, E., Ivanov, M., Blinova, V., 2007. The replacement of aragonite by authigenic carbonates (in the mud diapiric ridges, the Gulf of Cadiz) Geophys. Res. Abstr. 9, Abstr. 06912.
León, R., Somoza, L., Ivanov, M.K., Díaz-del-Río, V., Lobato, A., Hernández-Molina, F.J., Fernández-Puga, M.C., Maestro, A., Medialdea, T., Alveirinho, J., Vázquez, J.T., 2001. Seabed morphology and gas venting in the Gulf of Cadiz mud volcano area: imagery of multibeam data and ultra-high resolution data. Final Proc. Int. Conf. Geological Processes on Deep-Water European Margins, Moscow, Russia. UNESCO IOC Workshop Report, vol. 175, pp. 43–45.
León, R., Somoza, L., Medialdea, T., Maestro, A., Díaz-del-Río, V., Fernández-Puga, M.C., 2006. Classification of deep sea-floor features associated with methane seeps along the Gulf of Cadiz continental margin. Deep Sea Res. Part II 53, 1464–1481.
León, R., Somoza, L., Medialdea, T., González, F.J., Díaz-del-Río, V., Fernández-Puga, M.C., Maestro, A., Mata, M.P., 2007. Sea-floor features related to hydrocarbon seeps in deepwater carbonate-mud mounds of the Gulf of Cadiz: from mud flows to carbonate precipitates. Geo Mar. Lett. 27, 237–247.
Lonergan, L., White, N., 1997. Origin of the Betic-Rif mountain belt. Tectonics 16, 504–522.
Lyle, M., 1981. Formation and growth of ferromanganese oxides on the Nazca plate. In: Kulm, L.D., Dymond, J., Dasch, E.J., Hussong, D.M. (Eds.), Nazca Plate: crustal formation and Andean convergence. Geol. Soc. Am. Mem., vol. 154, pp. 269–293.
Maestro, A., Somoza, L., Medialdea, T., Talbot, C.J., Lowrie, A., Vázquez, J.T., Díaz-del-Río, V., 2003. Large scale slope failure involving Triassic and Middle Miocene salt and shale in the Gulf of Cadiz (Atlantic Iberian Margin). Terra Nova 15, 380–391.
Magalhães, V.H., Pinheiro, L.M., Ivanov, M., 2005. Methane-derived authigenic carbonates in the Gulf of Cadiz: cartography, distribution and controls. Eos Trans. AGU 86 (52), Fall Meet. Suppl., Abstr. OS33C-1484.
Maldonado, A., Somoza, L., Pallarés, L., 1999. The Betic Orogen and the Iberian–african boundary in the Gulf of Cadiz: geological evolution (central North Atlantic). Mar. Geol. 155, 9–43.
Manheim, F.T., Lane-Bostwick, C.M., 1988. Cobalt in ferromanganese crusts as a monitor of hydrothermal discharge on the Pacific sea floor. Nature 335, 59–62.
Martín-Puertas, C., Fernández-Puga, M.C., Mata, M.P., Vázquez Garrido, J.T., Díaz-del-Río, V., Somoza, L., 2006. Naturaleza de la brecha fangosa de volcanes de fango del Golfo de Cádiz: sistema diapírico del Guadalquivir y zona Tasyo. Rev. Soc. Geol. de España 19 (3–4), 257–270.
Medialdea, T., Vegas, R., Somoza, L., Vázquez, J.T., Maldonado, A., Díaz-del-Río, V., Maestro, A., Córdoba, D., Fernández-Puga, M.C., 2004. Structure and evolution of the "Olistostrome" complex of the Gibraltar Arc in the Gulf of Cadiz (eastern Central Atlantic): evidence from two long seismic cross-sections. Mar. Geol. 209 (1–4), 173–198.
Mottl, M.J., Wheat, C.G., Baker, E., Becker, N., Davis, E., Feely, R., Grehan, A., Kadko, D., Lilley, M., Massoth, G., Moyer, C., Sansone, F., 1998. Warm springs discovered on 3.5 Ma oceanic crust, eastern flank of the Juan de Fuca Ridge. Geology 26, 51–54.
Murray, J., Renard, A.F., 1891. Deep-sea deposits. Reports of the Scientific Results Explor. Voyage Challenger. 525 pp.
Nealson, K.H., Myers, C.R., 1992. Microbial reduction of manganese and iron: new approaches to carbon cycling. Appl. Environ. Microbiol. 58–2, 439–443.
Nicholson, K., Hein, J.R., Bühn, B., Dasgupta, S., 1997. Manganese Mineralization: Geochemistry and Mineralogy of Terrestrial and Marine Deposits. Special Publication Geological Society of London, vol. 119. London. 370 pp.
Niemann, H., Duarte, J., Hensen, C., Omoregie, E., Magalh, ães, V.H., Elvert, M., Pinheiro, L.M., Kopf, A., Boetius, A., 2006. Microbial methane turnover at mud volcanoes of the Gulf of Cadiz. Geochim. Cosmochim. Acta 70 (21), 5336–5355.
Palma, J.J.C., Pessanha, I.B.M., 2000. Depósitos ferromanganesíferos de océano profundo. Braz. J. Geophys. 18 (3), 431–446.
Peckmann, J., Reimer, A., Luth, U., Luth, C., Hansen, B.T., Heinicke, C., Hoefs, J., Reitner, J., 2001. Methane-derived carbonates and authigenic pyrite from the northwestern Black Sea. Mar. Geol. 177, 129–150.
Pinheiro, L.M., Ivanov, M.K., Sautkin, A., Akhmanov, G., Magalhães, V.H., Volkonskaya, A., Monteiro, J.H., Somoza, L., Gardner, J., Hamouni, N., Cunha, M.R., 2003. Mud volcanism in the Gulf of Cadiz: results from the TTR-10 cruise. Mar. Geol. 195, 131–151.
Raab, W.J., Meylan, M.A., 1977. Morphology. In: Glasby, G.P. (Ed.), Marine manganese deposits. Elsevier Oceanography Series, Amsterdam, pp. 109–146.
Reyss, J.L., Marchig, V., Ku, T.L., 1982. Rapid growth of a deep-sea manganese nodule. Nature 295 (5848), 401–403.
Riaza, C., Martínez del Olmo, W., 1996. Depositional model of the Guadalquivir-Gulf of Cadiz Tertiary basin. In: Friend, P.F., Dabrio, C.J. (Eds.), Tertiary basin of Spain: the stratigraphic record of crustal kinematics. Cambridge University Press, pp. 330–338.
Robinson, B.W., Kusakabe, M., 1975. Quantitative separation of sulphur dioxide for 34S/32S analyses from sulphides by combustion with cuprous oxide. Anal. Chem. 47, 1179–1181.
Rona, P., 2002. Marine minerals for the 21st century. Episodes 25, 2–12.
Rona, P., 2003. Resources of the sea floor. Science 299, 673–674.
Royden, L.H., 1993. The tectonic expression of slab pull at continental convergent boundaries. Tectonics 12, 303–325.
Somoza, L., Gardner, J.M., Díaz-del-Río, V., Vázquez, J.T., Pinheiro, L., Hernández-Molina, F.J., TASYO scientific parties, 2002. Numerous Methane Gas-related sea floor structures identified in Gulf of Cadiz. EOS Transactions, v. 83 (47), 541–543. Am. Geophys. Union.
Somoza, L., Díaz-del-Río, V., León, R., Ivanov, M., Fernández-Puga, M.C., Gardner, J.M., Hernández-Molina, F.J., Pinheiro, L.M., Rodero, J., Lobato, A., Maestro, A., Vázquez, J.T., Medialdea, T., Fernández-Salas, L.M., 2003. Seabed morphology and hydrocarbon seepage in the Gulf of Cadiz mud volcano area: acoustic imagery, multibeam and ultra-high resolution seismic data. Mar. Geol. 195, 153–176.
Stakes, D.S., Orange, D., Paduan, J.B., Salamy, K.A., Maher, N., 1999. Cold-seeps and authigenic carbonate formation in Monterey Bay. California. Mar. Geol. 159, 93–109.
Stadnitskaia, A., Ivanov, M.K., Blinova, V., Kreulen, R., van Weering, T.C.E., 2006. Molecular and carbon isotopic variability of hydrocarbon gases from mud volcanoes in the Gulf of Cadiz, NE Atlantic. Mar. Pet. Geol. 23, 281–296.
Stein, L.Y., La Duc, M.T., Grundl, T.J., Nealson, K.H., 2001. Bacterial and archaeal populations associated with freshwater ferromanganese micronodules and sediments. Environ. Microbiol. 3 (1), 10–18.
Torelli, L., Sartori, R., Zitellini, N., 1997. The giant chaotic body in the Atlantic Ocean of Gibraltar: new results from a deep seismic reflection survey. Mar. Pet. Geol. 14 (2), 125–138.
Verlaan, P.A., Cronan, D.S., Morgan, C.L., 2005. A comparative analysis of compositional variations in and between marine ferromanganese nodules and crusts in the South Pacific and their environmental controls. Prog. Oceanogr. 63, 125–158.
Volkov, I.I., 1979. Ferromanganese nodules. Oceanologiya, Khimiya Okeana, v. 2, Geokhimiya Donnykh Osadkov, pp. 414–467.
Von Stackelberg, U., 1997. Growth history of manganese nodules and crust of the Peru Basin. In: Nicholson, K., Hein, J.R., Bühn, B., Dasgupta, S. (Eds.), Manganese Mineralization: Geochemistry and Mineralogy of Terrestrial and Marine Deposits. Special Publication Geological Society of London, vol. 119, pp. 153–176. London.
Von Stackelberg, U., 2000. Manganese nodules of the Peru Basin. In: Cronan, D.S. (Ed.), Handbook of marine mineral deposits. CRC Press, pp. 197–238.
Walters, L.J., Claypool, G.E., Choquette, Ph.W., 1972. Reaction rates and d 18 O variation for the carbonate-phosphoric acid preparation method. Geochim. Cosmochim. Acta 36, 129–140.
Zhamoida, V.A., Butylin, V.P., Glasby, G.P., Popova, I.A., 1996. The nature of ferromanganese concretions from the Eastern Gulf of Finland, Baltic Sea. Mar. Georesour. Geotechnol. 14, 161–175.